IEEE Access
Multidisciplinary | Rapid Review | Open Access Journal

Received 8 May 2024, accepted 11 June 2024, date of publication 17 June 2024, date of current version 25 June 2024.

*Digital Object Identifier 10.1109/ACCESS.2024.3415960*

STANDARDS

# SRS Interference Management in TDD CJT for 5G

**KARTHIK MURALIDHAR[1], YOUNGROK JANG[2], YOUNSUN KIM[2], (Senior Member, IEEE), DIWAKAR SHARMA[1], HYOUNG-JU JI[2], (Senior Member, IEEE), SANTANU MONDAL[1], DATTARAJ DILEEP RAUT MULGAONKAR[1], SATYA KUMAR VANKAYALA[1], (Senior Member, IEEE), AND SEONGMOK LIM[2]**

[1]Samsung Research and Development Institute, Bengaluru 560037, India
[2]Samsung Research, Samsung Electronics, Seoul 06765, South Korea

Corresponding author: Karthik Muralidhar (karthik.mr@samsung.com)

**ABSTRACT** One of the work items in fifth generation (5G) radio layer 1 (RAN1) in the Release-18 third-generation partnership project (3GPP) standardization activity concerns sounding reference signal (SRS) enhancements to deal with interference management in time-division duplex (TDD) coherent joint transmission (CJT) for multiple transmission reception points (multiple TRPs or mTRP). The work item proposed to study two approaches: 1) interference randomization techniques (IRT) and 2) capacity enhancements (CE) of SRS. This paper discusses this work item in detail along with the authors' contributions to it. This paper can be broadly divided into three parts. In the first part, we provide an overview of the various techniques discussed by different companies in the standards. In the second part, we present our contribution of a novel SRS receiver with enhanced SRS capacity. We show how our improved SRS receiver allows the transmission of six SRSs over 12 subcarriers, which results in better performance (greater than 5 dB gain) than a conventional SRS receiver that supports only four SRSs over 12 subcarriers, as per the existing 3GPP standard. Capacity improvement is achieved by enabling closer placement of the SRS in the cyclic shift (CS) domain, which depends on leakage. Conventional SRS receivers are based on discrete Fourier transform (DFT), which have more leakages than the proposed Slepian-based SRS receiver, which has fewer leakages. We analysed in detail the effects of both DFT and Slepian on leakages in the CS domain. This capacity and/or performance improvement allows more user equipments (UEs) to simultaneously transmit SRS, allowing lower uplink transmission power to attain the same performance as conventional SRS receivers, thereby improving coverage. We investigate the changes that need to be implemented in existing standards to support such receivers, which can achieve an enhanced SRS capacity. In the third part, we present three novel enhancement techniques, that we proposed, namely, per-port cyclic shift (PP-CS) allocation scheme, CS hopping in a subset and muting of SRS transmission. CS hopping in a subset was accepted in 5G RAN1 Release-18 3GPP standardization activity as a means of reducing interference in TDD CJT for mTRP. In the section on simulation results in this paper, we show that there is a distinct improvement in performance (compared to existing legacy systems) when CS hopping is employed. This is because, in the CS domain, as the CS associated with a user hops across orthogonal frequency-division multiplexing (OFDM) symbols, it has different neighbouring users in different symbols and leakages due to these neighbours get reduced as the channel estimates are averaged over different OFDM symbols. We demonstrate that it is possible to mitigate almost all interference and reach the zero-interference lower bound of a single TRP (sTRP) case with a combination of PP-CS, CS hopping in a subset, and muting of SRS transmission. The key idea is to recognize that the extra propagation distance (EPD) of UEs from other TRPs results in higher frequency selectivity in the channel. To address this, we designed efficient SRS CS resource-allocation strategies.

**INDEX TERMS** 3GPP release-18, 5G RAN1, capacity enhancements, discrete prolate spheroidal sequence (Slepian), interference randomization, SRS enhancements.

The associate editor coordinating the review of this manuscript and approving it for publication was Filbert Juwono.

## I. INTRODUCTION

ONE of the methods to improve cellular performance is to have a greater number of base stations and smaller cell sizes to ensure better coverage. Traditionally, we had one base station per cell that catered to all the users in that cell. Cell-free massive multiple-input multiple-output (MIMO) technology is a promising technology for meeting the requirements of a high number of users and higher data rates in 5G networks [1], [2]. As shown in [1] and [2], cell-free massive MIMO has better performance than the conventional one base station per cell concept. The idea is to have a large number of access points (APs) distributed across the cell, catering to all users via joint coherent signal processing. In the literature, cell-free massive MIMO is also known as ''network MIMO,'' ''distributed MIMO,'' ''Coordinated Multi-Point (CoMP)'' and ''distributed antenna systems (DAS).'' In the context of 5G, mTRPs act as APs in implementing cell-free massive MIMO technology [3].

In [4] and [5], the authors discussed that interference in uplink pilots (pilot contamination) is one of the main limiting factors of massive MIMO systems. Good channel estimates of SRS (an uplink pilot channel in 5G) in the TDD CJT and mTRP scenarios are very important for realizing as much of the gains as promised by cell-free massive MIMO. SRS in 5G is used by UEs in the uplink to sound the uplink channel so that the TRP can learn the uplink channel and use it for a variety of purposes, such as scheduling, positioning, and coarse uplink channel estimation. The SRS consists of a root sequence called the Zadoff-Chu (ZC) sequence multiplied by a complex exponential sequence transmitted over the SRS subcarriers [6]. In TDD CJT systems [3], there are multiple TRPs in a cell with each TRP associated with a set of UEs that it serves. The UEs can be either a single-port or multi-port. The SRS CS resources for these UEs are reused across TRPs (while the root sequence may be the same); thus there is interference among the SRS of various UEs received by a TRP. To realize the aforementioned benefits, RAN1 Release-18 3GPP standardization assigned a work item to study the topic of managing interference [7]. In [7], *SRS enhancement to manage inter-TRP cross-SRS interference targeting TDD CJT via SRS capacity enhancement and/or interference randomization was mentioned, with the following constraints: 1) without consuming additional resources for SRS, 2) reuse existing SRS comb structure, and 3) without new SRS root sequences*. Therefore, two studies were, conducted: i) IRT and ii) CE of SRS.

We now discuss IRT and CE methods. We begin by discussing the TDD CJT in the context of the mTRP scenario. In Fig. 1, we consider two TRPs (TRP1 and TRP2), $UE_{1,1}$ is associated with and served by TRP1. Likewise, $UE_{2,1}$ is associated with and served by TRP2. In general, $UE_{i,j}$ denotes the $j$th UE associated with the $i$th TRP or the $j$th port of a UE associated with the $i$th TRP, as the case may be. We study the signals at TRP1 only and call $UE_{1,1}$ the desired UE and $UE_{2,1}$ the interfering UE. The purpose of IRT methods is to minimize the interference experienced by $UE_{1,1}$'s SRS received at TRP1 owing to $UE_{2,1}$'s SRS received at TRP1. Various methods have been discussed in the standards, such as increasing the maximum number of CSs (the current values in existing standards [6] are six, eight, and 12), time-domain orthogonal cover code (TD-OCC), muting, finer CS granularity, CS and comb offset hopping in a subset, the per-port CS (PP-CS) allocation scheme, and configuring the sequence index. All of these schemes are presented and discussed in Sec. III. Of these methods, we have made contributions to CS hopping in a subset, the PP-CS allocation scheme, and muting, which will be discussed in detail in Sec. IV. We show in Sec. V, a combination of these three methods can achieve a lower bound in the performance corresponding to the case of a no-interference scenario or sTRP.

Next, we discuss the CE method. It depends mainly on the receiver at the TRP. If an intelligent receiver at the TRP can support more users (enhanced SRS capacity) over a given set of SRS subcarriers, then we should appropriately change the specifications in the standards to support such a receiver in the TRP (the specifications should allow transmission of the increased number of users). We present the design of such an intelligent receiver in detail in Sec. II. PP-CS allocation is one such scheme that can support SRS receivers with enhanced capacities. The PP-CS allocation scheme is discussed in detail in Sec. III-F, Sec. IV and Sec. V.

A brief summary of the various methods in Release-18 standardization, along with their associated references, is presented in Table 1. Furthermore, a flowchart depicting the summary of the various schemes in this standardization activity of Release-18 is shown in Fig. 2 (where red fonts and boxes correspond to our contribution). A brief description of the SRS in 5G is provided in Sec. I-B, and the design of the conventional SRS receiver is presented in Sec. I-C. We present our novel SRS 5G receiver with enhanced capacity in Sec. II. A brief discussion of the standardization support of such receivers with enhanced SRS capacity is given in Sec. II-F. An overview of the various IRT schemes discussed in Release-18 is presented in Sec. III. Our contributions to the IRT schemes and simulation results are presented in Sec. IV and Sec. V, respectively.

### A. RELATED WORKS AND CONTRIBUTIONS

In [3], a detailed discussion of SRS interference for TDD CJT systems in the context of the mTRP is presented. They discussed that the current interference suppression method whitens the colored interference by low correlation sequences during least squares operation at the base station. However, the sequence correlation would be quite large, especially for a short sequence length, which may incur large interference. For example, the sequence length would be very limited if frequency hopping is performed for coverage enhancement. This issue is more serious in the CJT scenario. Fig. 6 in [3] shows how interference arises in such cases. If a channel in the frequency domain is multiplied by a complex exponential

**TABLE 1. Summary of various schemes in Release-18, associated references and their descriptions.**

| Sl. No. | Scheme | Brief description | References | Location in this paper |
|---|---|---|---|---|
| 1 | Increasing maximum number of CSs | Currently the maximum CS $n_{\text{SRS}}^{\text{CS,max}} = 6, 8, 12$ as per existing standards [6]. Increasing this value beyond 12 can result in capacity enhancements which was one of the objectives of this work item in Release-18 [7]. | [25], [26], [27], [28] | Sec. III-A |
| 2 | TD-OCC | Currently in existing standards [6], the complex exponential sequence characterized by a CS can be viewed as an OCC in frequency domain, that allows many SRSs to occupy the same set of SRS subcarriers. In existing standards the frequency-domain SRS is repeated over $N_{\text{symb}}^{\text{SRS}}$ time domain symbols. Instead of mere repetition, TD-OCC proposes to have an OCC over these $N_{\text{symb}}^{\text{SRS}}$ time domain symbols. | [34], [35], [36] | Sec. III-B |
| 3 | Muting | Muting is to desist from transmitting SRS on some SRS occasions as per some rule. | [31], [29], [32] | Sec. III-C, Sec. IV-C |
| 4 | Finer CS granularity | Currently the $\alpha_i$ in the standards [6] is given by $\alpha_i = 2\pi \frac{n_{\text{SRS}}^{\text{CS,i}}}{n_{\text{SRS}}^{\text{CS,max}}}$. It is proposed to add the term $2\pi \frac{n_{\text{SRS}}^{\text{CS,offset}}}{2n_{\text{SRS}}^{\text{CS,max}}}$ to $\alpha_i$. So for $n_{\text{SRS}}^{\text{CS,max}} = 8$, in the existing standards the CSs are $0, 1, 2, 3, \ldots, 7$, but in the proposed standards, the CSs could be $0, 0.5, 1, 1.5, \ldots, 7.5$, i.e., CSs could be fractional with a granularity of 0.5. | [30] | Sec. III-D |
| 5 | CS and comb offset hopping | In the existing standards [6], the CS $n_{\text{SRS}}^{\text{CS,i}}$ and comb offset $\bar{k}_0^{(p_i)}$ are constant across the $N_{\text{symb}}^{\text{SRS}}$ SRS OFDM symbols. In Release-18 it is proposed to change these values over the $N_{\text{symb}}^{\text{SRS}}$ SRS OFDM symbols. This hopping scheme is expected to randomize and reduce interference. | [39], [30], [37], [38], [32] | Sec. III-E, Sec. IV-C |
| 6 | PP-CS allocation | In the current standards [6] the CSs of an $N_{\text{ap}}$-port UE is equally divided in the range $0, \ldots, n_{\text{SRS}}^{\text{CS,max}} - 1$. While this is suited for a sTRP, it might not be suitable for a mTRP, where we need to assign CS values individually for each port of the UE and they might not be equidistant over the range of $0, \ldots, n_{\text{SRS}}^{\text{CS,max}} - 1$ for better performance. | [29], [40], [32] | Sec. III-F, Sec. IV |
| 7 | Configuring sequence index | In existing standards [6], 60 different base sequences with low cross-correlation are defined when SRS sequence length is equal to or larger than 72 bits by $u = 0, \ldots, 29$ and $v = 0, 1$. However, when sequence hopping is not configured, currently $v$ is always fixed to 0. The proposal in Release-18 is to use $v = 1$ as well. | [29] | Sec. III-G |

sequence, it results in a shift in the effective time domain delays. The advantages of CS hopping in the context of legacy systems and in the frequency domain were discussed in [3] by analysing the power delay profile (PDP) of the effective delays in the delay domain. In our paper, we also analyse the CS hopping in the context of legacy systems and frequency domain, by noting that the the interference is mainly due to leakages in CS domain and by CS hopping, we have different neighbours in the CS domain in different SRS symbols and leakages due to these different neighbours is considerably reduced as channel estimates is averaged over the different SRS symbols. Note that many companies also proposed CS hopping in the context of legacy systems, as can be seen from the fifth column and fourth row in Table 1. CS hopping in the context of legacy systems was eventually accepted in 3GPP RAN1 standardization. Finally, in this paper, we also propose and discuss the CS hopping scheme in the context of the PP-CS scheme, which is associated with better performance than CS hopping in the context of legacy systems, as can be seen later in Sec. V.

Prior to Release-18, SRS was primarily used for sTRP operations [6]. With that in mind, the CSs associated with various ports of a multi-port UE were such that the CSs were evenly distributed in the CS domain (more about this later in Sec. I-B) over the allowed CS values, as in [8], [9], [10], and [11], although at times, it was used in an mTRP-like scenario [8]. The equidistant CSs were designed to have the maximum distance between two neighbouring CS values, which resulted in less interference. However, in an mTRP scenario, this CS allocation scheme is suboptimal for handling the interference. This is because the EPD is involved between the TRPs. Keeping this in mind, we propose a new CS allocation scheme, called PP-CS, that helps manage interference better and considerably improves performance. The PP-CS scheme is discussed in detail in Sec. IV. Based on the findings of the PP-CS scheme, we suggest a new muting scheme in Sec. IV. Together with the CS hopping, PP-CS, and muting schemes, we demonstrate that we can achieve a performance close to that of an sTRP (lower bound of no interference) in Sec. V.

CoMP in LTE-Advanced (LTE-A) is similar to mTRP in 5G. The method to address the interference in CoMP for LTE-A is discussed in detail in [8]. They discussed three methods, namely, CS coordination, CoMP coordination and TD-OCC enhancements of SRS. TD-OCC was one of the schemes that was discussed and debated in 3GPP Release-18.

An interference mitigation scheme based on a precoded SRS was described in [9]. Precoding allows the change of the signal subspace of the effective precoded channel, provides flexibility to align different precoded SRS signals in different signal subspaces, and helps in the management of the interference. Apart from the mTRP CJT scenario, there are other scenarios for SRS interference management. In [10], SRS interference was managed in the context of mobile satellite communication systems, where large inter-beam and intra-beam interference destroyed the orthogonality for SRS from different users, resulting in a low received signal to noise ratio (SNR). 3GPP 5G also uses SRS for positioning. The SRS received by many TRPs helps determine the position of a UE. In [11], the mitigation of interference of SRS when used for positioning purposes is described in detail.

As mentioned previously, the channel in the frequency domain corresponds to a set of delays in the delay domain (channel impulse response or CIR). The effective delay spread is greater than the actual delay spread, as we are dealing with a finite number of SRS subcarriers. This is due to the windowing effect, and reduces as we increase the observation window. However, the exponential sequences (or CSs) used to multiplex various SRSs are such that the corresponding delays (effective delay spread) in the delay domain of these SRSs do not overlap. This effective delay spread determines the capacity or the number of SRSs that can be multiplexed in the frequency domain. If the effective delay spread is greater, this naturally leads to reduced capacity. In [12], the occurrence of the CIR energy leakage problem in DFT receivers was mentioned, as discussed above. They proposed reducing leakages using frequency domain windows such as Hanning, Hamming or Blackman. Views similar to [12] are also presented in [13]. The contents of this paragraph is discussed in detail in Sec. II-C. Therefore, to increase the capacity (and/or performance), leakages must be minimized. Slepian sequences [14], [15], [16], [17], [18], [19] are known to have the least leakages, and we use this to improve capacity and present a Slepian-based receiver in Sec. II. Slepian sequences are good at modelling low-pass signals. Very often, we encounter band-pass signals. In the context of SRS, the effective channel becomes band-pass due to the choice of CSs, as will be seen in Sec. I-C. In such cases, as discussed in [20], we have to down convert the band-pass signal to low-pass before modelling by the Slepian basis, as will be discussed in Sec. II-C and Sec. II-D. Other related references for capacity improvement of SRS are given in [21] and [22].

Our contributions in this paper can be summarized as below.

1) **3GPP proposal summary**: We provide a brief summary of the various proposals discussed in 3GPP by various companies for the work item in question along with our contributions. This is discussed further in Sec. III.
2) **New SRS receiver**: We propose a new SRS receiver based on Slepian sequences, instead of the conventional DFT-based SRS receiver. This is discussed in detail in Sec. II. We developed the motivation for a Slepian-based SRS receiver, as the Slepian sequence is associated with the least leakages. On the other hand, DFT is associated with significant leakages and is also associated with the Gibb's phenomenon. Owing to this, we will eventually show in Sec. V, the proposed Slepian-based SRS receiver has more than 50% capacity improvement compared to the conventional DFT-based 3GPP receiver, and this is achieved with a gain of more than 5 dB.
3) **PP-CS scheme**: We propose the concept of PP-CS scheme. This is discussed further in Sec. IV. This was shown to be optimal in the case of the mTRP TDD CJT scenario, as it considers the EPD of the UEs from other TRPs.
4) **CS hopping**: We propose the CS hopping scheme, both in the context of legacy system and PP-CS schemes. This is discussed further in Sec. IV.CS hopping improves performance in the context of both legacy and the proposed PP-CS schemes, as will be discussed in detail in Sec. V.
5) **Muting scheme**: We propose the muting scheme in Sec. IV. Together with the PP-CS and CS hopping schemes, we show in Fig. 25 that the mTRP TDD CJT scenario can achieve almost the same performance as the sTRP case (no interference, lower bound).

*Notations:* Modulo operation is denoted as mod and $k \bmod N$ is denoted as $\grave{k}_N$. Element-wise matrix multiplication is denoted by $\circ$. The expectation operator is defined as $E\{.\}$. Identity matrix is denoted by $\mathbf{I}$. Bold upper case denotes matrices, bold lower case denotes vectors and normal fonts denote scalar quantities. The quantity $\mathcal{D}(\mathbf{x})$ is a diagonal matrix with $\mathbf{x}$ along the main diagonal. The conjugate of a vector $\mathbf{x}$ is denoted by $\mathbf{x}^*$. We define an $N \times 1$ vector $\mathbf{f}_{a,N} = [\,1 \;\; e^{j2\pi\frac{a}{N}} \;\; e^{j2\pi\frac{2a}{N}} \;\; \ldots \;\; e^{j2\pi\frac{a(N-1)}{N}}\,]^T$. If $N$ is understood from the context, we just use $\mathbf{f}_a$ and drop the Subscript $N$. The quantity $\mathbf{x}(a)$ denotes the $a$th element of $\mathbf{x}$ and $\mathbf{X}(a,b)$ is the element of $\mathbf{X}$ in the $a$th row and $b$th column. The quantity $\lfloor x \rfloor$ denotes the greatest integer less than or equal to $x$, which is commonly called *floor* operation. A brief note of the notations used for the ports of desired and interfering UEs. Let $d_a$ denote the $a$th desired single-port UE (or the $a$th port of the desired UE in the case of a multi-port UE) and $i_a$ denote the $a$th interfering single-port UE (or the $a$th port of the interfering UE in the case of a multi-port UE). When we say $d_a = p$, it means CS $p$ is assigned to $d_a$ (the same holds for $i_a$ as well).

### B. SRS IN 5G NEW RADIO (NR)

Fig. 3 shows the SRS structure. As per [6], the UE has $N_{\text{ap}}^{\text{SRS}}$ antenna ports $p_i$, $i = 0, \ldots N_{\text{ap}}^{\text{SRS}} - 1$. The SRS is repeated across $N_{\text{symb}}^{\text{SRS}}$ continuous orthogonal frequency-division multiplexing (OFDM) symbols in a slot, where The SRS starts at the $l_0$th OFDM symbol where $l_0 = 13 - l_{\text{offset}}$ and $l_{\text{offset}} \in \{0, \ldots, 13\}$ (the SRS symbols are indexed from

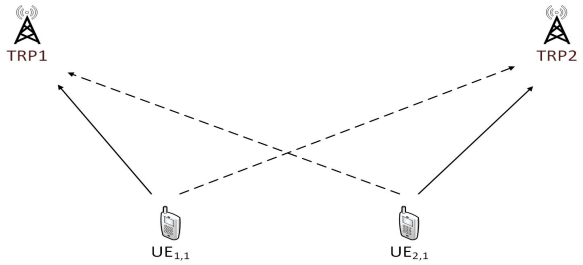


**FIGURE 1.** Scenario of TDD CJT in mTRP.

zero and there are 14 OFDM symbols in a slot). The SRS resource elements (REs) or subcarriers of one user in an OFDM symbol are spaced $K_{\text{TC}}$ apart and are said to be in the comb. There are $K_{\text{TC}}$ such combs. Each comb can carry one or more SRSs (These SRSs are assigned different CSs). The value mapped to the $n$th SRS RE in the $l'$th OFDM symbol for the $p_i$th port is given by

$$r^{(p_i)}(n, l') = r_{u,v}^{(\alpha_i,\delta)}(n) = e^{j\alpha_i n}\bar{r}_{u,v}(n) \tag{1}$$

where $0 \le n \le M_{\text{sc,b}}^{\text{SRS}} - 1$, $l' \in \{0, \ldots, N_{\text{symb}}^{\text{SRS}} - 1\}$, $M_{\text{sc,b}}^{\text{SRS}}$ is the number of SRS REs, $\bar{r}_{u,v}(n)$ is the ZC sequence with group number $u$, sequence number $v$, $\delta = \log_2(K_{\text{TC}})$, $e^{j\alpha_i n}$ is the CS exponential and

$$\alpha_i = 2\pi \frac{n_{\text{SRS}}^{\text{CS, i}}}{n_{\text{SRS}}^{\text{CS, max}}}. \tag{2}$$

In the above equation, we say that the CS associated with the $p_i$th port is $n_{\text{SRS}}^{\text{CS, i}}$ and the maximum CS value is $n_{\text{SRS}}^{\text{CS, max}}$. This is a slight deviation from [6], where they call $\alpha_i$ is the CS and $n_{\text{SRS}}^{\text{CS, max}}$ is the maximum number of CSs.

If $N_{\text{ap}}^{\text{SRS}} = 4$, $n_{\text{SRS}}^{\text{CS, max}} = 6$, the quantity $n_{\text{SRS}}^{\text{CS, i}}$ in (2) is given by

$$n_{\text{SRS}}^{\text{CS, i}} = \left( n_{\text{SRS}}^{\text{CS}} + \frac{n_{\text{SRS}}^{\text{CS, max}} \lfloor \frac{(p_i - 1000)}{2} \rfloor}{N_{\text{ap}}^{\text{SRS}}/2} \right) \bmod n_{\text{SRS}}^{\text{CS, max}} \tag{3}$$

If the condition $N_{\text{ap}}^{\text{SRS}} = 4$, $n_{\text{SRS}}^{\text{CS, max}} = 6$ is not satisfied, the quantity $n_{\text{SRS}}^{\text{CS, i}}$ in (2) is given by

$$n_{\text{SRS}}^{\text{CS, i}} = \left( n_{\text{SRS}}^{\text{CS}} + \frac{n_{\text{SRS}}^{\text{CS, max}}(p_i - 1000)}{N_{\text{ap}}^{\text{SRS}}} \right) \bmod n_{\text{SRS}}^{\text{CS, max}} \tag{4}$$

where $n_{\text{SRS}}^{\text{CS}} \in 0, \ldots, n_{\text{SRS}}^{\text{CS, max}} - 1$ is contained in the higher layer parameter *transmissionComb*. As per the above equations, the CSs are evenly distributed across the allowable CS values of $0, \ldots, n_{\text{SRS}}^{\text{CS, max}} - 1$. In case (3), the four ports are divided into two duplicate sets of two CSs each. Each set was evenly distributed across $0, \ldots, n_{\text{SRS}}^{\text{CS, max}} - 1$. Furthermore, as described in [6], both sets of CSs were allocated to two different combs. In (4), all the CSs are evenly distributed across $0, \ldots, n_{\text{SRS}}^{\text{CS, max}} - 1$.

This even distribution of CSs means that if the CS of the first port of a UE is fixed, the CSs of all other ports of that UE are also fixed and equidistant from one another over $0, \ldots, n_{\text{SRS}}^{\text{CS, max}} - 1$. This has some potential disadvantages, which are discussed in detail in Sec. III-F and Sec. IV. In these sections, we propose that it is sometimes advantageous to configure the CSs of each port of the UE, which is called the PP-CS scheme.

When SRS is transmitted on a given SRS resource, the sequence $r^{(p_i)}(n, l')$ for each OFDM symbol $l'$ and for each of the antenna ports of the SRS resource, is multiplied by the amplitude scaling factor $\beta_{\text{SRS}}$ and mapped in sequence starting with $r^{(p_i)}(0, l')$ to REs $(k, l)$ in a slot for each of the antenna ports $p_i$ according to

$$a_{K_{\text{TC}}k' + k_0^{(p_i)}, l' + l_0}^{(p_i)} = \frac{1}{\sqrt{N_{\text{ap}}}} \beta_{\text{SRS}} r^{(p_i)}(k', l') \tag{5}$$

for $k' = 0, \ldots, M_{\text{sc,b}}^{\text{SRS}} - 1$ and $l' = 0, \ldots, N_{\text{symb}}^{\text{SRS}} - 1$. The frequency domain starting position $k_0^{(p_i)}$ is defined as

$$k_0^{(p_i)} = \bar{k}_0^{(p_i)} + n_{\text{offset}}^{\text{FH}} + n_{\text{offset}}^{\text{RPFS}} \tag{6}$$

where

$$\bar{k}_0^{(p_i)} = n_{\text{shift}} N_{\text{sc}}^{\text{RB}} + \left( k_{\text{TC}}^{(p_i)} + k_{\text{offset}}^{l'} \right) \bmod K_{\text{TC}} \tag{7}$$

where $n_{\text{offset}}^{\text{FH}}, n_{\text{offset}}^{\text{RPFS}}, n_{\text{shift}}, N_{\text{sc}}^{\text{RB}}, k_{\text{TC}}^{(p_i)}, k_{\text{offset}}^{l'}$ are all defined in [6].

### C. CONVENTIONAL SRS RECEIVER

In this section, we describe how many users (or multiple ports of a user) can be transmitted and multiplexed in the same frequency region, and how the channels of those users can be estimated using conventional SRS receivers. Consider an $N \times 1$ vector of received SRS subcarriers $\mathbf{y}$. For simplicity and ease of understanding, we depict $N_U = 2$ users. The frequency-domain SRS channel (across $N$ subcarriers) of $i$th user is denoted as $\mathbf{h}_i$. The channel is a low-pass signal and its fast Fourier transform (FFT) has only a few low-pass FFT bins (around the DC or zeroth FFT bin). We can approximate the channel as

$$\mathbf{h}_i = \frac{1}{N} \sum_{k=-w}^{w} \mathbf{h}_i^{(F)}(\check{k}_N) \mathbf{f}_{\check{k}_N} \tag{8}$$

where vector $\mathbf{h}_i^{(F)}$ is the FFT of $\mathbf{h}_i$. This is depicted in Fig. 4, where the FFT of low-pass channel $\mathbf{h}_i$ has only a few low-pass bins ($w$ low-pass bins on either side of the DC bin). Among all the FFT bins of the channel, only these low-pass bins have appreciable energy and can be used to reconstruct the channel with a good degree of accuracy. The first user transmits $\mathbf{f}_0$ across the $N$ subcarriers and the second user transmits $\mathbf{f}_{\frac{N}{2}}$ across the same set of $N$ subcarriers. Furthermore, we assume that $\frac{N}{2} - w > w$ and $\frac{N}{2} + w < N - w$. With this assumption and the transmission choice of the two users ($\mathbf{f}_0$ and $\mathbf{f}_{\frac{N}{2}}$), we can safely assume that the FFT bins with appreciable energy of the channel of both users do not overlap, as shown in Fig. 4. Using (8) and the preceding discussion, the received signal $\mathbf{y}$

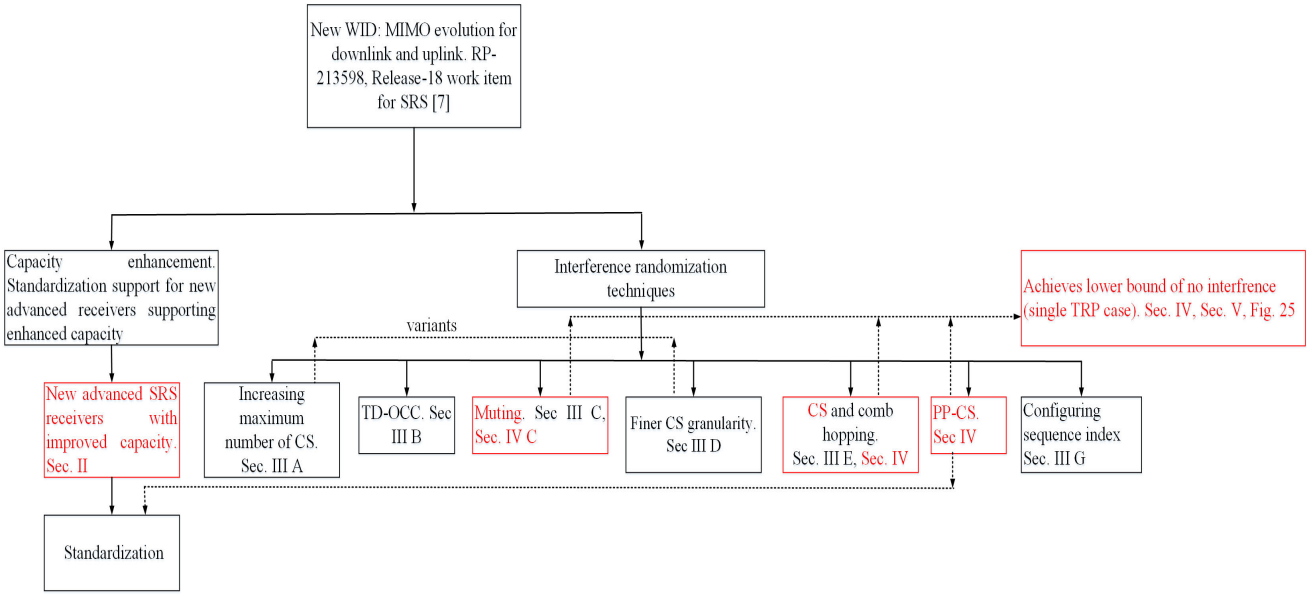


**FIGURE 2.** Pictorial depiction of overview, organization and authors' contributions for SRS work item in Release-18 3GPP standardization. Authors' contributions are in red font/boxes.

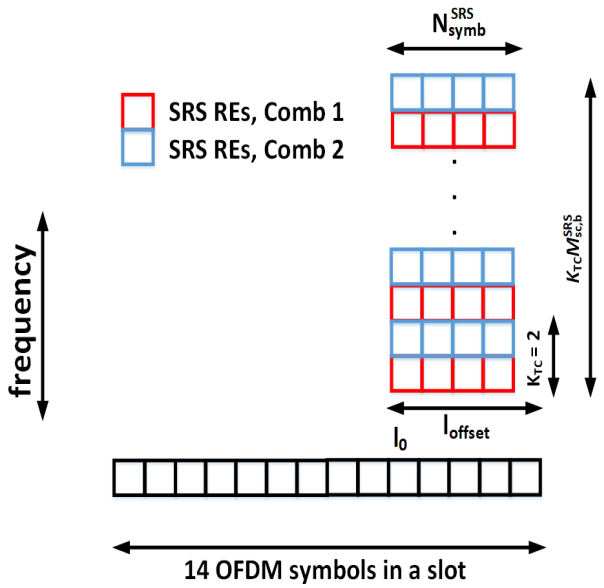


**FIGURE 3.** SRS structure in 5G.

is given by (neglecting the noise),

$$\begin{aligned}\mathbf{y} &= \mathbf{h}_1 \circ \mathbf{f}_0 + \mathbf{h}_2 \circ \mathbf{f}_{\frac{N}{2}} \\ &= \frac{1}{N}\sum_{k=-w}^{w} \mathbf{h}_1^{(F)}(\check{k}_N)\mathbf{f}_{\check{k}_N} + \frac{1}{N}\sum_{k=-w}^{w} \mathbf{h}_2^{(F)}(\check{k}_N)\mathbf{f}_{(\frac{N}{2}+\check{k})_N}.\end{aligned} \tag{9}$$

For simplicity, we neglect the ZC sequence. Let the FFT of $\mathbf{y}$ be denoted by the vector $\mathbf{y}^{(F)}$. Each FFT bin of is approximately equal to the corresponding FFT bin of the channel for one user. Various $\mathbf{h}_i^{(F)}(.)$ are estimated as follows

$$\begin{aligned}\mathbf{h}_1^{(F)}(a) &= \mathbf{y}^{(F)}(a), \quad a \in \{0, \ldots, w, N-w, \ldots, N-1\} \\ \mathbf{h}_1^{(F)}(a) &= 0, \quad a \in \{w+1 \ldots, N-w-1\} \\ \mathbf{h}_2^{(F)}(a) &= \mathbf{y}^{(F)}(a), \quad a \in \{\frac{N}{2}-w, \ldots, \frac{N}{2}+w\} \\ \mathbf{h}_2^{(F)}(a) &= 0, \quad a \notin \{\frac{N}{2}-w, \ldots, \frac{N}{2}+w\}.\end{aligned} \tag{10}$$

Once the $\mathbf{h}_i^{(F)}(.)$ are estimated as per the above equation, the channels $\mathbf{h}_i$ can be estimated as per (8).

## II. CAPACITY ENHANCEMENT VIA ADVANCED RECEIVERS

In this section, we present a new SRS receiver with enhanced capacity. In a multi-user SRS receiver, we typically build a linear model to model the many channels of all users, followed by the minimum mean square estimation (MMSE) of the various channels [12]. This model typically employs a DFT basis. In Sec. II-A, we study how other bases, such as Slepian [14], [15], [16], [17], [18], [19] and polynomial basis [23], impact the SRS receiver performance. In particular, we study the performance of the receiver in terms of the number of model parameters required for each basis, and establish the relationship between the number of SRSs and the number of model parameters. The DFT, Slepian, and polynomial basis are described in detail in Sec. II-B. In particular, we discuss the important property of the Slepian sequence which has the most concentrated energy in a given bandwidth and the least leakage of energy outside the given bandwidth. This is used in Fig. 9 in Sec. II-C to show that the perceived bandwidth of estimates of a small number of signal samples based on projections to a Slepian subspace does not increase appreciably compared to the signal's true

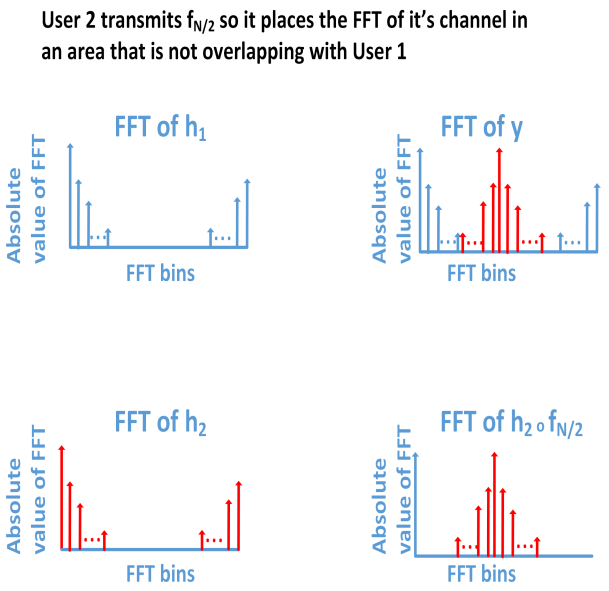


**FIGURE 4.** Depiction of FFT of two SRS users multiplexed in frequency. FFT bins of the channels of both users with appreciable energy do not overlap and can be recovered and channels of both users easily reconstructed. The x-axis refers to FFT bins and y-axis refers to absolute value of FFT.

bandwidth. This is in sharp contrast to the usually observed case, where the perceived bandwidth of estimates of a small number of signal samples based on projections to a DFT subspace increases appreciably as compared to the signal's true bandwidth owing to the windowing effect. The perceived bandwidth is important in the sense that the capacity of the number of supported SRSs increases with a decrease in the perceived bandwidth of one SRS. In Sec. II-C, we also show via Fig. 7 and Fig. 8, that $N$ samples of a low-pass signal band limited between $-\epsilon$ and $\epsilon$ lies in a subspace spanned by $\lceil 2N\epsilon \rceil + 2$ Slepian basis vectors only [14].

### A. STUDY OF BASIS

A slowly varying signal can be approximated by projection onto a basis matrix. The approximation and reconstruction depend on the choice of basis. The conventional SRS receiver is based on the DFT [12] and has the problem of Gibbs phenomenon [12], where the channel estimates at the edge of a region have a lot of error. This is illustrated in Fig. 5. It can be seen that channel estimation using the DFT basis is affected by the Gibbs phenomenon, while Slepian [14], [15], [16], [17], [18], [19] and polynomial basis [23], [24] are immune to it.

Let $\mathbf{y}$ be an $N \times 1$ SRS channel vector (SRS over $N$ subcarriers or REs). We assumed only one SRS. Let us consider an $N \times R$ ($R \ll N$) basis matrix $\boldsymbol{\Phi}$ and an $R \times 1$ basis coefficient vector $\mathbf{x}$. We approximate $\mathbf{y}$ as $\mathbf{y} \approx \boldsymbol{\Phi}\mathbf{x}$. Note that for the DFT and Slepian basis, $\boldsymbol{\Phi}$ is a unitary matrix and $\boldsymbol{\Phi}^H\boldsymbol{\Phi} = \mathbf{I}$, an identity matrix. The quantity $\mathbf{x}$ was estimated as $\hat{\mathbf{x}} = \boldsymbol{\Phi}^H\mathbf{y}$. For the polynomial basis [23], [24], the basis matrix $\boldsymbol{\Phi}$ is not unitary, and $\mathbf{x}$ is estimated as $\hat{\mathbf{x}} = (\boldsymbol{\Phi}^H\boldsymbol{\Phi})^{-1}\boldsymbol{\Phi}^H\mathbf{y}$. The channel estimate was given by $\hat{\mathbf{y}} = \boldsymbol{\Phi}\hat{\mathbf{x}}$.

Now, we examine how good the channel estimate $\hat{\mathbf{y}}$ is for each of the bases as a function of $R$. Define $\boldsymbol{\Phi}_M^{(R)}$ as the first $R$ columns of basis matrix $\boldsymbol{\Phi}$ where the choice of basis $M$ could be one of $F$, $S$ and $P$ (for DFT or Fourier, Slepian and polynomial). Similarly, $\mathbf{x}_M^{(R)}$ denotes the first $R$ elements of $\mathbf{x}$. Channel reconstruction error for each of the bases is defined as

$$\rho_M^{(R)} = \frac{\|\mathbf{y} - \boldsymbol{\Phi}_M^{(R)}\mathbf{x}_M^{(R)}\|^2}{\mathbf{y}^H\mathbf{y}}. \tag{11}$$

Note that for the Fourier and Slepian basis $\|\mathbf{y}\|^2 = \|\mathbf{x}\|^2$ because $\boldsymbol{\Phi}$ is a unitary matrix, but for the polynomial basis $\|\mathbf{y}\|^2 \approx \|\mathbf{x}\|^2$ as $\boldsymbol{\Phi}$ is not a unitary matrix. Ideally, for a good modelling of the channel we require $\|\mathbf{x}_M^{(R)}\|^2 \approx \|\mathbf{x}\|^2$ for small values of $R$. For capacity enhancement, smaller values of $R$ are preferred as we have $N_U R \leq N$, where $N_U$ SRSs/UEs/ports are multiplexed over the same set of subcarriers with different CSs. Furthermore, we define the quantity

$$\beta_M^{(R)} = \frac{\|\mathbf{x}_M^{(R)}\|^2}{\|\mathbf{x}\|^2}. \tag{12}$$

For any basis, if $\beta_M^{(R)}$ reaches unity for small values of $R$ then it is a good basis. In summary, the following two features determine the choice of basis $M$:

- $\beta_M^{(R)}$ tends to unity for smaller values of $R$.
- $\rho_M^{(R)}$ decreases for small values of $R$.

It can be seen from Fig. 6 that we need more basis coefficients at a higher reconstruction error for the Fourier basis than for the polynomial and Slepian basis, that is, $\rho_S^{(R_S)} < \rho_F^{(R_F)}$ and $\rho_P^{(R_P)} < \rho_F^{(R_F)}$ for $R_P < R_F$ and $R_S < R_F$ where $R_M$ is the value of $R$ for Method $M$. Lower values of $R$ for better performance also means that capacity $N_U$ is increased as $N_U R \leq N$. Therefore, the choice of basis becomes very important for both performance improvement and capacity enhancement and it is shown that a Slepian/polynomial basis is much better than a Fourier (DFT) basis. However, this is not the end of the story. A good basis is of no use if it has a higher complexity. We show that the complexity of a Slepian/polynomial-based SRS receiver is similar to that of a DFT-based receiver in Sec. II-E.

### B. BASIS MATRIX $\Phi$

We now briefly discuss the DFT, polynomial, and Slepian bases. For the DFT basis, we have $\boldsymbol{\Phi}(i,j) = e^{\frac{j2\pi ij}{N}}$, $0 \leq i,j \leq N-1$. For polynomial basis, the first column of $\boldsymbol{\Phi}$ is constant, the second column is linear, the third is parabolic, etc. In particular, for the polynomial basis, $\boldsymbol{\Phi}(i,j) = (i+1)^j$, $0 \leq i,j \leq N-1$. Slepian sequences are provided in [14], [15], [16], [17], [18], and [19]. In MATLAB, they can be generated using the command *dpss*. We now briefly explain Slepian or discrete prolate spheroidal sequences (dpss). Consider a finite

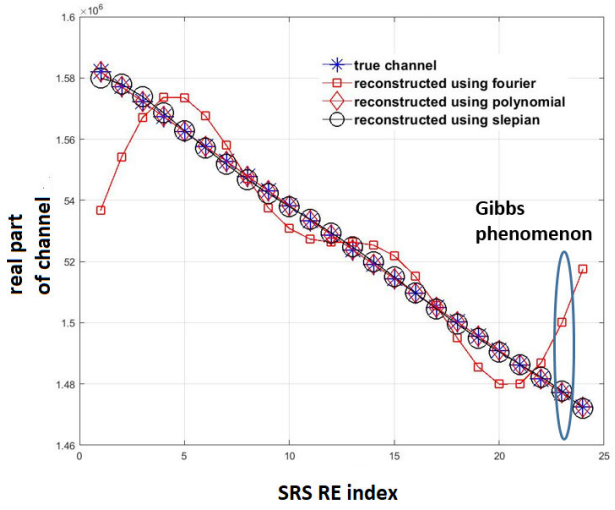


**FIGURE 5.** Channel estimation using Fourier basis is affected by Gibbs phenomenon, whereas channel estimation by Slepian and polynomial basis are immune to it. Parameters are CDL-B, delay spread = 30 ns, carrier frequency = 3.5 GHz, $K_{TC} = 2$ and subcarrier spacing is 15 kHz.

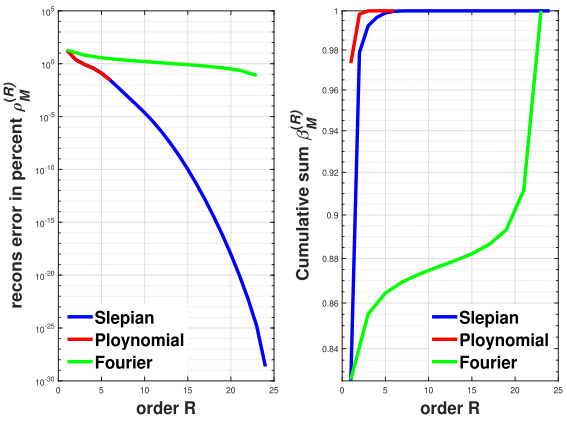


**FIGURE 6.** Modelling performance of different basis. CDL-C, delay spread = 100 ns, $K_{TC} = 4$, subcarrier spacing = 30 kHz, $N = 24$.

sequence $x(n)$ of $N$ samples, the DFT of which is given by

$$X(f) = \sum_{0}^{N-1} x(n) e^{-j2\pi fn}. \tag{13}$$

Note that $X(f)$ is defined over the interval $(-0.5, 0.5)$ and is periodic with a period of unity. We wish to find sequences with the maximum energy concentration in the region $(-\omega, \omega), 0 \leq \omega < 0.5$, that is, sequences that maximize $\sigma(N, \omega)$ where

$$\sigma(N, \omega) = \frac{\int_{-\omega}^{\omega} |X(f)|^2 df}{\int_{-0.5}^{0.5} |X(f)|^2 df}. \tag{14}$$

Slepian sequences maximize $\sigma(N, \omega)$. Note that as per the definition of (14), maximising $\sigma(N, \omega)$, corresponds to minimizing $|X(f)|^2$ outside the range $(-\omega, \omega)$, which can

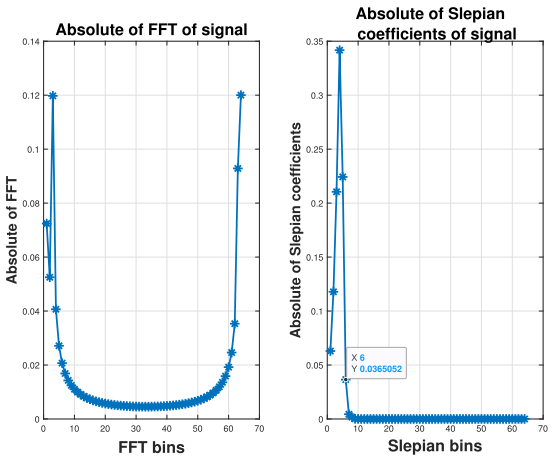


**FIGURE 7.** Depiction of $N$ samples of a low-pass signal band limited between $-\epsilon$ and $\epsilon$ lies in a subspace spanned by approximately $\lceil 2N\epsilon \rceil + 2$ dominant Slepian basis vectors. $N = 64, \epsilon = \frac{2}{64}$. A Slepian bin corresponds to a Slepian basis vector and the y-axis is the absolute value of the Slepian coefficient associated with that Slepian basis vector.

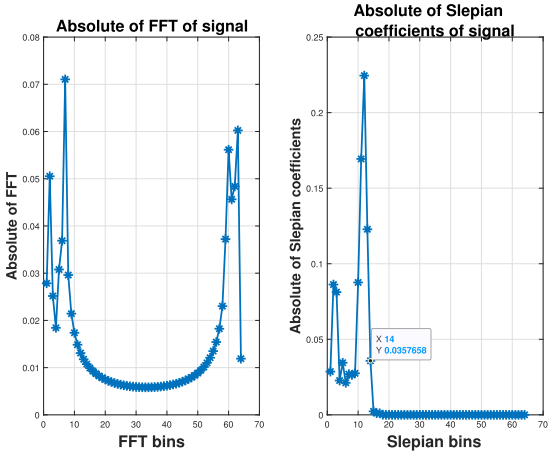


**FIGURE 8.** Depiction of $N$ samples of a low-pass signal band limited between $-\epsilon$ and $\epsilon$ lies in a subspace spanned by approximately $\lceil 2N\epsilon \rceil + 2$ dominant Slepian basis vectors. $N = 64, \epsilon = \frac{6}{64}$. A Slepian bin corresponds to a Slepian basis vector and the y-axis is the absolute value of the Slepian coefficient associated with that Slepian basis vector.

be termed leakage. Consequently, Slepian sequences have minimum leakages outside $(-\omega, \omega), 0 \leq \omega < 0.5$. This will be useful in discussions in Sec. II-C, in the context of Fig. 9.

### C. FURTHER INFORMATION ON SLEPIAN BASIS

If we consider $N$ samples of a channel (which essentially is a low-pass signal) in time or frequency (across OFDM subcarriers) band limited between $-\epsilon$ and $\epsilon$ and if we project it onto a subspace spanned by the Slepian basis, then approximately $2N\epsilon$ Slepian basis coefficients have appreciable energy. In other words, the $N \times 1$ low-pass signal lies in a subspace spanned by $2N\epsilon$ Slepian vectors. This can be observed in Figs. 7 and 8, where we can see that the left side of the figure has absolute (abs.) values of FFT coefficients and the right side of the figure has absolute

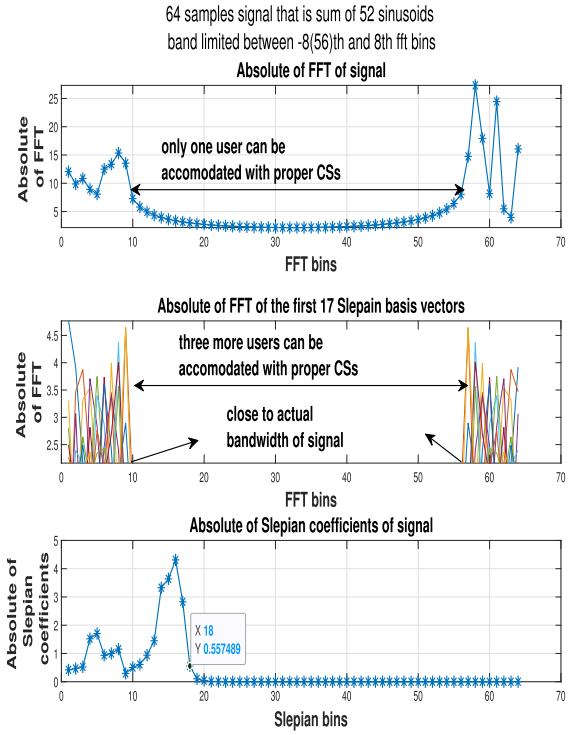


**FIGURE 9.** The perceived bandwidth of a small number of samples of a low-pass signal apparently increases for DFT-based estimates, thereby reducing capacity and performance. This does not occur for Slepian-based estimates, thereby enhancing capacity and performance.

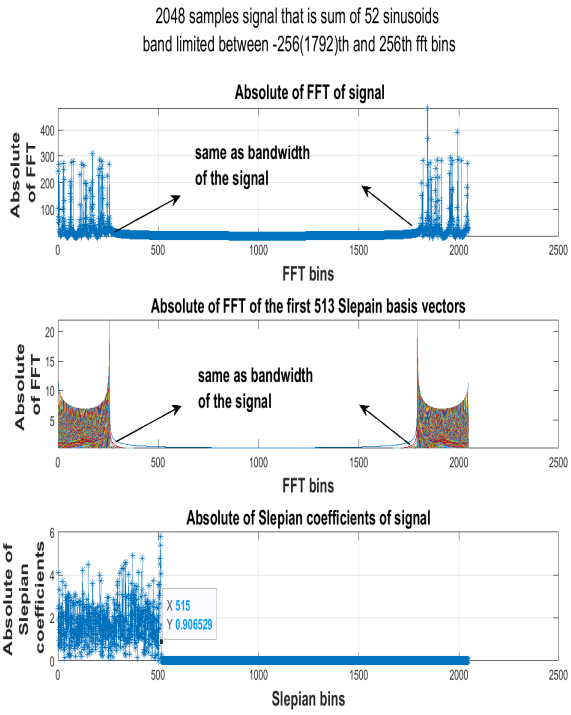


**FIGURE 10.** The perceived bandwidth of a large number of samples of a low-pass signal does not change for both DFT-based and Slepian-based estimates.

values of Slepian basis coefficients and that the number of Slepian basis coefficients is approximately $2N\epsilon$ ($\lceil 2N\epsilon \rceil + 2$ to be precise [14]). Furthermore, the number of Slepian basis

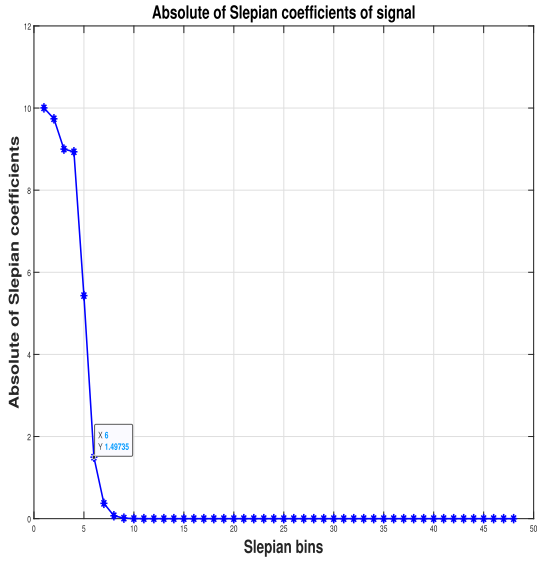


**FIGURE 11.** Study of Slepian basis in SRS context. Forty eight SRS subcarriers $N = 48$ (no subcarriers are skipped for simplicity, i.e., $K_{\mathrm{TC}} = 1$), $D_O = \{0T_C, 9T_C, 18T_C, 27T_C, 36T_C\}$. The quantity $d_l$ is from a normal distribution $\mathcal{N}(0, 1)$. Parameters are $N_{\mathrm{SC}} = 512$, $\epsilon = \frac{18}{512}$, $\kappa = -\frac{18}{512}$, $\lceil 2N\epsilon \rceil + 2 = 6$.

coefficients with appreciable energy is far less than that of DFT basis coefficients ($R_S < R_F$).

Motivated by the above facts, we now analyse the capacity enhancement with the Slepian basis. How many signals can be multiplexed such that they can be recovered from their sum (the details of the recovery are given in Sec. II-D) effectively? We see above that each signal can be characterized by $R_S = 2N\epsilon$ Slepian basis coefficient vectors, and if there are $N_U$ such signals, we have $R_S N_U < N$ or

$$N_U = \frac{N}{R_S} = \frac{N}{2N\epsilon} = \frac{1}{2\epsilon} \tag{15}$$

which is essentially the number of signals, each with a bandwidth of $2\epsilon$, that can be accommodated over the allowable normalized digital frequency range $0 < f < 1$, such that their spectra do not overlap. Recall that for discrete signals, the frequency is the normalized digital frequency (dimensionless) which is the product of the analog frequency (Hz) and sampling duration (in time and units as seconds). The normalized digital frequency is between 0 and 1 (or -0.5 to 0.5). Furthermore, we look at an alternate way of arriving at the above results. In Fig. 9, we have $N = 64$ samples of a low-pass signal band limited between $-\epsilon$ and $\epsilon$ with a bandwidth $B = 2\epsilon$ where $\epsilon = \frac{8}{64}$. The signal is the sum of 52 complex sinusoids. The perceived bandwidth via FFT (upper figure in Fig. 9) is $B_P = 2\bar{\epsilon}$ where $\bar{\epsilon} > \epsilon$. The capacity in this case is

$$N_{U,F} = \frac{1}{B_P} = \frac{1}{2\bar{\epsilon}}. \tag{16}$$

It can be seen that $\lceil 2N\epsilon \rceil + 2 = 18$ Slepian basis coefficients are enough to model this signal (lower figure in Fig. 9) and the

FFT of each of these 18 Slepian basis figures has a bandwidth almost equal to the true bandwidth, i.e., $B_T = 2\epsilon$ (This follows from the definition of Slepian sequences in Sec. II-B after (14)). Consequently, the capacity while using Slepian is

$$N_{U,S} = \frac{1}{B_T} = \frac{1}{2\epsilon} \tag{17}$$

which is close to the true capacity, and $N_{U,S} > N_{U,F}$. Note that (15) and (17) are the same.

The perceived bandwidth increases because of the finite samples in the observation owing to windowing. Consider the FFT of $N$ samples of a single sinusoid $e^{j2\pi kn}$ (for $k$ not a multiple of $\frac{1}{N}$). Because this is just one frequency, we should expect only one nonzero FFT bin. Not really. For small values of $N$, there will be many nonzero FFT bins in the shape of a sinc function, the width of which decreases as $N$ increases. This is true as $N \to \infty$ when the width of the sinc tends to zero; thus the FFT has only one nonzero FFT bin. Therefore, we revisit the observations in the previous paragraph for a large number of samples $N$, as depicted in Fig. 10. Here, we consider $N = 2048$ samples. We can see that even for FFT, the perceived bandwidth is close to the true bandwidth, and we can conclude that $N_{U,S} \approx N_{U,F}$. Therefore, the Slepian basis is helpful for modelling low-pass signals with a small number of observations.

We now examine SRS signals in the context of the above discussion. For simplicity, we consider contiguous SRS subcarriers or $K_{\text{TC}} = 1$. Considering $N$ SRS subcarriers packed into the $N \times 1$ vector $\mathbf{y}$, the $k$th SRS subcarrier is the $k$th RE for simplicity, and the channel at the $k$th SRS subcarrier is given by

$$\mathbf{y}(k) = \sum_{\tau_l \in D_O} d_l e^{-j2\pi k \Delta f \tau_l} \tag{18}$$

where $D_O$ is the set of all the multipath timing offsets, $\tau_l$ is the timing offset of the $l$th path, $d_l$ is the associated multipath amplitude, and $\Delta f$ is the subcarrier spacing. Furthermore, $\Delta f = \frac{1}{T} = \frac{1}{N_{\text{SC}} T_C}$ where the OFDM symbol duration is $T$ and $N_{\text{SC}}$ is the number of chips or samples per OFDM symbol, with the chip duration being $T_C$. The cardinality of the Set $D_O$ is denoted by $|D_O|$. This means as per (18), the SRS vector $\mathbf{y}$ consists of $|D_O|$ complex exponentials that are band limited between $-\Delta f D_{O,\min}$ and $-\Delta f D_{O,\max}$ where $D_{O,\min}$ and $D_{O,\max}$ are the minimum and maximum values of the timing offsets in the Set $D_O$. Now, let us multiply $\mathbf{y}$ by an exponential sequence $e^{-j2\pi\kappa k}$ to yield $\tilde{\mathbf{y}}$, such that $\tilde{\mathbf{y}}$ is band-limited between $-\epsilon$ and $\epsilon$ (so that it becomes a low-pass signal), where

$$\begin{aligned} \epsilon &= \frac{\Delta f D_{O,\max} - \Delta f D_{O,\min}}{2} \\ \kappa &= \frac{-\Delta f D_{O,\max} - \Delta f D_{O,\min}}{2}. \end{aligned} \tag{19}$$

So now if we project $\tilde{\mathbf{y}}$ on to a Slepian basis subspace, the subspace will effectively be spanned by $\lceil 2N\epsilon \rceil + 2$ Slepian basis vectors only, similar to Fig. 7 and Fig. 8. An example of this is shown in Fig. 11.

### D. PROPOSED RECEIVERS

We assume $N_U$ users/SRSs/ports use the same time-frequency resources. Let $\mathbf{y}$ be the observed vector over $N$ SRS REs or subcarriers. Let the channel vector of the $i$th user be denoted by an $N \times 1$ vector $\mathbf{h}_i$ which is given by

$$\mathbf{h}_i = \boldsymbol{\Phi}_M^{(R)} \mathbf{x}_M^{(R,i)}. \tag{20}$$

where the basis coefficient vector $\mathbf{x}_M^{(R)}$ for the $i$th user is $\mathbf{x}_M^{(R,i)}$. Define $\mathbf{A}$ as

$$\mathbf{A} = \left[ \mathbf{R}_1 \boldsymbol{\Phi}_M^{(R)} \ , \ldots , \ \mathbf{R}_{N_U} \boldsymbol{\Phi}_M^{(R)} \right] \tag{21}$$

and the concatenation of basis coefficient vectors of all users as

$$\mathbf{x}_{\text{all}} = \begin{bmatrix} \mathbf{x}_M^{(R,1)} \\ \vdots \\ \mathbf{x}_M^{(R,N_U)} \end{bmatrix}. \tag{22}$$

We have $\mathbf{y} \approx \mathbf{A}\mathbf{x}_{\text{all}}$. The quantity $\mathbf{R}_i$ is an $N \times N$ diagonal matrix with a reference sequence (ZC sequence and CS exponential from (1)) of the $i$th user along the diagonal. Here, $\mathbf{Z}$ is an $N \times N$ diagonal matrix with a ZC sequence along the diagonal. Let $\mathbf{E}_i$ be a diagonal matrix with CS exponential sequence of the $i$th user along the main diagonal. We have $\mathbf{R}_i = \mathbf{Z}\mathbf{E}_i$. Normally, matrix $\mathbf{Z}$ in $\mathbf{R}_1, \ldots, \mathbf{R}_{N_U}$ is the same for all users in the cell. We denote $\bar{\mathbf{A}} = \mathbf{Z}^H \mathbf{A}$ and $\bar{\mathbf{y}} = \mathbf{Z}^H \mathbf{y}$. Note that the $\mathbf{R}_1, \ldots, \mathbf{R}_{N_U}$ in $\mathbf{A}$ if constructed without ZC sequence and only with exponential CSs, then it becomes $\bar{\mathbf{A}}$. Because the ZC sequence is the same across all users, we have $\bar{\mathbf{y}} \approx \bar{\mathbf{A}}\mathbf{x}_{\text{all}}$. An estimate of $\mathbf{x}_{\text{all}}$ is given by

$$\hat{\mathbf{x}}_{\text{all}} = (\bar{\mathbf{A}}^H \bar{\mathbf{A}})^{-1} \bar{\mathbf{A}}^H \mathbf{y}. \tag{23}$$

Using (20), (22), and (23), one can estimate the channel of all users $\mathbf{h}_i$, $i = 1, \ldots, N_U$. The proposed receiver uses Slepian sequences for $\boldsymbol{\Phi}_M^{(R)}$.

### E. COMPLEXITY DISCUSSIONS

The key to estimating the channel $\mathbf{h}_i$ of all $N_U$ users is (23). Therefore, we spend some time analysing $\bar{\mathbf{A}}$. Let us assume that all the CSs of $N_U$ users are equidistant (a very common practice) within region $0, \ldots, n_{\text{SRS}}^{\text{CS,max}} - 1$. The CS of the $i$th user is $n_{\text{SRS}}^{\text{CS},i} = B + (i-1)\Delta$ where $\Delta = \frac{n_{\text{SRS}}^{\text{CS,max}}}{N_U}$, and $0 \le B \le \Delta - 1$. Note that we have the following identities

$$\begin{aligned} \mathbf{Z}^H \mathbf{Z} &= \mathbf{I} \\ \mathcal{D}(\mathbf{f}_k)\mathcal{D}(\mathbf{f}_k)^H &= \mathbf{I} \\ \mathbf{E}_k &= \mathcal{D}(\mathbf{f}_B)\mathcal{D}(\mathbf{f}_{(k-1)\Delta}) \end{aligned} \tag{24}$$

using which we simplify $\bar{\mathbf{A}}$ as

$$\begin{aligned} \bar{\mathbf{A}} &= \mathbf{Z}^H \mathbf{A} \\ &= \mathbf{Z}^H \mathbf{Z} \left[ \mathbf{E}_1 \boldsymbol{\Phi}_M^{(R)} \ , \ldots , \ \mathbf{E}_{N_U} \boldsymbol{\Phi}_M^{(R)} \right] \qquad (25) \\ &= \left[ \mathbf{E}_1 \boldsymbol{\Phi}_M^{(R)} \ , \ldots , \ \mathbf{E}_{N_U} \boldsymbol{\Phi}_M^{(R)} \right] \\ &= \mathcal{D}(\mathbf{f}_B)\mathbf{M} \qquad (26) \end{aligned}$$

where

$$\mathbf{M} = \left[\mathcal{D}(\mathbf{f}_0)\boldsymbol{\Phi}_M^{(R)}, \ldots, \mathcal{D}(\mathbf{f}_{(N_U-1)\Delta})\boldsymbol{\Phi}_M^{(R)}\right]. \quad (27)$$

It should be noted that $\mathbf{M}$ is independent of the choice of CSs for the $N_U$ users (as long as the equidistant criterion is satisfied). We have

$$\bar{\mathbf{A}}^H\bar{\mathbf{A}} = \mathbf{M}^H\mathbf{M} \quad (28)$$

which also turns out to be independent of the choice of CSs for the $N_U$ users. Consequently, $(\bar{\mathbf{A}}^H\bar{\mathbf{A}})^{-1}$ is also independent of the choice of CSs. For a given length $N$ of SRS, the quantity can be precomputed and stored. Furthermore, $\bar{\mathbf{A}}^H = \mathbf{M}^H\mathcal{D}(\mathbf{f}_B^*)$ which can be easily computed for any choice of $B$ (any set of equidistant CSs). Hence $(\bar{\mathbf{A}}^H\bar{\mathbf{A}})^{-1}\bar{\mathbf{A}}^H$ in (23) does not depend on the choice of $B$ and can be precomputed and used.

Note that the structure of (8) (for the conventional SRS receiver) and (20) (for the proposed SRS receiver) are identical. In both equations, $\mathbf{h}_i$ is computed by multiplying an $N \times R_M$ matrix by an $R_M \times 1$ vector. In (8), $R_M = 2w$ whereas in (20) $R_M = R_S$. The $2w$ is equivalent to $R_F$ in Sec. II-A and $R_S < 2w$. Similarly, (10) (for the conventional SRS receiver and considering the FFT computation of $\mathbf{y}^{(F)}$) and (23) (for the proposed SRS receiver) are similar. Hence, the complexities of the proposed and conventional receivers are of the same order. In particular, because $R_S < 2w$, the complexity of the proposed receiver is less than that of a conventional receiver.

### F. STANDARDIZATION SUPPORT FOR ADVANCED SRS RECEIVERS

The advanced SRS receiver, discussed in Sec. II-D has an enhanced SRS capacity at a better performance compared to conventional DFT-based 3GPP SRS receivers in Sec. I-C, as shown in Fig. 27. In the figure, the advanced SRS receiver of this section supports six SRSs over 12 SRS subcarriers ($n_{\text{SRS}}^{\text{CS,max}} = 12$) at a much better performance than a conventional DFT-based SRS receiver that supports only four SRSs, as per the standard. The six SRSs supported by the advanced SRS receiver in this section can be a combination of one four-port UE and another two-port UE. Note that the difference in the values of CSs of any two ports is a minimum of two. Such a scenario can never be supported by existing standards. In existing standards, one parameter from the higher layers determines the CS values of all ports of a UE, and they are equidistant over the allowable range of CSs. To support the four- and two-port UEs of the advanced receiver (with the constraint that no two CS values are consecutive), what we actually need in the standards is a PP-CS allocation scheme, where the CSs of each port of the UE are explicitly assigned/determined by higher layers. The PP-CS allocation scheme is discussed in detail in Sec. III-F and Sec. IV.

## III. INTERFERENCE RANDOMIZATION SCHEMES

In this section, we briefly present and discuss the various IRT schemes discussed in Release-18 3GPP standardization.

### A. INCREASING MAXIMUM NUMBER OF CSS

Currently, in the standards [6], three values of $n_{\text{SRS}}^{\text{CS, max}}$ are supported: $n_{\text{SRS}}^{\text{CS, max}} = 6, 8, 12$. Each value corresponds to one value of $K_{\text{TC}}$. The association values of $(K_{\text{TC}}, n_{\text{SRS}}^{\text{CS, max}})$ are (2, 8), (4, 12) and (8, 6). According to existing standards [6], the values of $(K_{\text{TC}}, n_{\text{SRS}}^{\text{CS, max}})$ were chosen depending on the frequency selectivity of the channel. In Release-18, [25], [26], [27], [28] dealt with the Tdoc contributions discussing this approach.

One of the objectives of this release with regard to this work item was capacity enhancement, with the following constraints:

- without consuming additional resources for SRS.
- reuse existing SRS comb structure.
- without new SRS root sequences.

It is indeed possible to enhance the capacity with the above constraints, which was the goal of Sec. II. From Sec. II-C, Figs. 9 and 10, it can be seen that if there is a large number of SRS subcarriers, the perceived bandwidth ($2\bar{\epsilon}$) of a SRS approaches it's true bandwidth $2\epsilon$. However, for a small number of SRS subcarriers, the perceived bandwidth is appreciably higher than the true bandwidth of SRS. The complex exponential sequences place the power spectral density (PSD) of each SRS such that it does not overlap. The number of SRSs that can be multiplexed (capacity) in the frequency domain is given by (15). Therefore, for a small number of SRS subcarriers, the capacity decreased, and the capacity increased with an increase in SRS subcarriers.

The above discussion clarifies that it is better to work with all $N$ SRS subcarriers when $N \gg n_{\text{SRS}}^{\text{CS, max}}$, rather than the conventional method of decoding the channel for every $n_{\text{SRS}}^{\text{CS, max}}$ SRS subcarriers. This naturally leads to working with increased CSs, which are more advantageous and enhance the capacity.

### B. TD-OCC

In existing standards [6], various SRS (different ports of a multi-port UE, many single-port UEs, or a combination of both) can occupy the same set of SRS subcarriers. The complex exponential sequence acts like an orthogonal cover code (OCC) and helps separate the effects of the channels of various SRSs. The SRS in frequency is repeated over time-domain OFDM symbols, as described in Sec. I-B. However, instead of mere repetition, we can multiply the SRS values for a given subcarrier and across time-domain OFDM symbols by an OCC in the time domain (TD-OCC) as well. This is the basic idea for extending the OCC to the time domain. This is better than time-division multiplexing (TDM). In TDM, different SRS occupy different time domain OFDM symbols. While it can be shown that the capacity for

TD-OCC is the same as TDM, there is a performance gain in TD-OCC with respect to TDM as the SRS in TD-OCC is spread over a greater number of time domain symbols and averaging reduces the effects of noise and improves the signal-to-noise ratio (SNR). Generally, TD-OCC helps in SRS that corresponds to the cell edge (or in this case between two TRPs).

For TD-OCC (5) is rewritten as under for

$$a^{(p_i)}_{K_{\mathrm{TC}}k'+k_0^{(p_i)},l'+l_0} = \frac{1}{\sqrt{N_{\mathrm{ap}}}}\beta_{\mathrm{SRS}}w^{(p_i)}(k',l')r^{(p_i)}(k',l') \quad (29)$$

for $k' = 0,\ldots,M^{\mathrm{SRS}}_{\mathrm{sc,b}}-1, l' = 0,\ldots,N^{\mathrm{SRS}}_{\mathrm{symb}}-1$. In the above equation, $w^{(p_i)}(k',l')$ is the TD-OCC for the $p_i$th port (or user), $k'$th SRS subcarrier, and $l'$th OFDM symbol. Let us concatenate the $w^{(p_i)}(k',l')$ for the $p_i$th port (or user), $k'$th SRS subcarrier, and all OFDM symbols into a TD-OCC vector as

$$\mathbf{w}^{(p_i,k')} = [w^{(p_i)}(k',0)\ldots \quad w^{(p_i)}(k',N^{\mathrm{SRS}}_{\mathrm{symb}}-1)]\cdot \quad (30)$$

Likewise, we can view $r^{(p_i)}(n,l')$ in (1) as a frequency-domain OCC (FD-OCC), which is characterized by $\alpha_i$. In compliance with the existing standards, we assume this to be constant across all SRS OFDM symbols.

Note that the TD-OCC vector needs to be orthogonal across ports and subcarriers, that is,

$$\mathbf{w}^{(p_i,k')}\mathbf{w}^{(p_j,m')H} = 0 \quad p_i \neq p_j,\ k' \neq m'\cdot \quad (31)$$

As regards the TD-OCC vector, it can have the following variations

- The TD-OCC vector is unique for all subcarriers for a given port.
- The TD-OCC vector is unique for a given subcarrier for a given port.
- The combination of the TD-OCC and FD-OCC vectors is unique for all subcarriers for a given port, and FD-OCC is unique for a given port.
- The combination of the TD-OCC and FD-OCC vectors is unique for a given subcarrier for a given port, and FD-OCC is unique for a given port.

In compliance with existing standards, we kept the FD-OCC vector the same across all SRS OFDM symbols. We do not consider the details of the receiver design for the various cases enumerated above.

### C. MUTING

One of the main proponents of muting was [29]. Therein, they described two approaches. Muting is a rule that decides whether or not to transmit SRS on an SRS occasion. Note that we also proposed a muting rule, the details of which are given in Sec. IV-C. Another one of our contributions is the PP-CS allocation described in Sec. III-F and Sec. IV. Note that the PP-CS allocation, along with the CS subset hopping described in Sec. III-E and our version of muting, as given in Sec. IV-C can account for almost all interferences

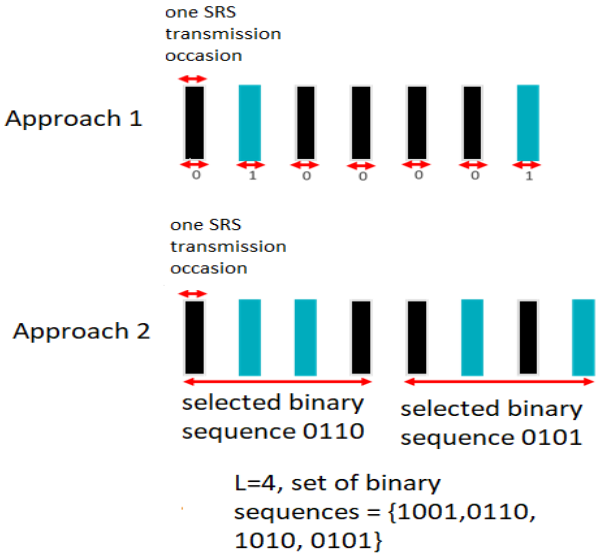


**FIGURE 12.** Muting scheme proposed in [29]. The figure is taken from [29].

and achieves a lower-bound performance of an sTRP. This is discussed extensively in Sec. IV.

We will briefly touch upon the muting scheme in [29]. An SRS transmission opportunity can be defined as a unit of transmission or muting. For example, the SRS transmission opportunity can be per OFDM symbol, per SRS resource, etc. Thus, there can be two approaches for pseudo-random muting of SRS, as explained below and illustrated in Fig. 12.

- Approach 1: The UE decides whether or not to transmit an SRS in a transmission opportunity according to a formula that is determined based on the pseudo-random sequence $c(i)$ as a function of time (e.g., slot number and symbol number). For a given SRS transmission opportunity, the formula generates either 0 or 1, which correspond to muting or transmission, respectively.
- Approach 2: The UE selects a binary sequence of length $L$ corresponding to $L$ SRS transmission opportunities according to a formula based on the pseudo-random sequence $c(i)$ as a function of time (e.g., slot or symbol number of the first SRS transmission opportunity). For a given L SRS transmission opportunities, the formula generates an index that points to a binary sequence of length $L$ from a set of binary sequences.

### D. FINER CS GRANULARITY

This scheme was proposed in [30]. Currently, $\alpha_i$ in the standards [6] is given by $\alpha_i = 2\pi\frac{n^{\mathrm{CS,i}}_{\mathrm{SRS}}}{n^{\mathrm{CS,max}}_{\mathrm{SRS}}}$. It is proposed to add the term $2\pi\frac{n^{\mathrm{CS,offset}}_{\mathrm{SRS}}}{2n^{\mathrm{CS,max}}_{\mathrm{SRS}}}$ to $\alpha_i$, where $0 \leq n^{\mathrm{CS,offset}}_{\mathrm{SRS}} \leq 2n^{\mathrm{CS,max}}_{\mathrm{SRS}} - 1$. For example, if $n^{\mathrm{CS,max}}_{\mathrm{SRS}} = 8$, in the existing standards, the CSs are $0, 1, 2, 3, \ldots, 7$, but in the proposed standards, the CSs could be $0, 0.5, 1, 1.5, \ldots, 7.5$, i.e., CSs could be fractional with a granularity of 0.5. In the upcoming

standards, this feature will be enabled only if the flag *cyclicShiftHoppingFinerGranularity* is configured.

This can be considered a variant of Sec. III-A. For a CS of, say 2.5 and $n_{\text{SRS}}^{\text{CS,max}} = 8$, $\alpha_i = 2\pi\frac{1.5}{8}$ which is equal to $\alpha_i = 2\pi\frac{3}{16}$ which corresponds to a CS of 3 and $n_{\text{SRS}}^{\text{CS,max}} = 16$ (the maximum CS is increased by a factor two to be equal to 16).

### E. CS AND COMB OFFSET HOPPING

In the existing standards [6], the CS $n_{\text{SRS}}^{\text{CS,i}}$ and comb offset $\bar{k}_0^{(p_i)}$ are constant across the $N_{\text{symb}}^{\text{SRS}}$ SRS OFDM symbols. This means that in each of the $N_{\text{symb}}^{\text{SRS}}$ OFDM symbols, the neighbours in the CS and comb domains for any SRS will be one and the same. Note that the channel estimates for an SRS are eventually averaged over $N_{\text{symb}}^{\text{SRS}}$ SRS symbols. By changing the neighbours for an SRS in both the CS and comb domains, as a function of the SRS OFDM symbol, the averaging of the channel estimate improves as each SRS sees a different neighbour, and hence different interference, in each SRS OFDM symbol. In Release-18, it was proposed to change the CS $n_{\text{SRS}}^{\text{CS,i}}$ and comb offset $\bar{k}_0^{(p_i)}$ values over the $N_{\text{symb}}^{\text{SRS}}$ SRS OFDM symbols. This hopping scheme is expected to randomize and reduce interference.

Note that in the existing standards [6], the CSs of all $N_{\text{ap}}$ ports of a UE are equidistant over $0, \ldots, n_{\text{SRS}}^{\text{CS,max}} - 1$. Therefore, even if CS hopping is employed, the effective CS values (denoted by $n_{\text{SRS, eff}}^{\text{CS,i}}$ for the $i$th port of the UE in a given OFDM symbol) between the $N_{\text{ap}}$ ports are expected to be equidistant over $0, \ldots, n_{\text{SRS}}^{\text{CS,max}} - 1$. This is the case if CS hopping is allowed over the entire allowable CS range of $0, \ldots, n_{\text{SRS}}^{\text{CS,max}} - 1$. Note that another CS hopping scheme was discussed and agreed upon in Release-18. This is CS hopping within a subset. This was done so that Release-18 UEs can be multiplexed with legacy UEs in the same comb, where legacy UEs CS values do not hop over SRS OFDM symbols. Whether to hop within a subset of CS values or not is configured using the parameter *cyclicShiftHoppingSubset*. When CS hopping in a subset is allowed, the effective CS values (denoted by $n_{\text{SRS, eff}}^{\text{CS,i}}$) between the $N_{\text{ap}}$ ports are also expected to be equidistant over $0, \ldots, n_{\text{SRS}}^{\text{CS,max}} - 1$ as well.

In the following, we discuss the above using an example. Consider $N_{\text{ap}} = 4$ and $n_{\text{SRS}}^{\text{CS,max}} = 8$. First, we assume that the *cyclicShiftHoppingSubset* is not configured, that is, CS does not hop within a subset. The hopping scheme is presented in Table 2. Note that a distance of three is maintained between CSs of any two ports of the UE while hopping. Let us assume that the flag *cyclicShiftHoppingSubset* is configured. We consider two two-port UEs. The CS hopping in a subset is presented in Table 3. UE1 is a legacy UE with no CS hopping and UE2 is a Release-18 UE whose CS hops in a subset. The subset of effective CSs is 2,3,4 and 5 for one port, and the other port is six CSs away.

The finer CS granularity scheme described in Sec. III-D is activated only when the parameter *cyclicShiftHoppingSubset*

**TABLE 2.** Example of CS hopping over the entire range of $0, \ldots, n_{\text{SRS}}^{\text{CS,max}} - 1$. The parameters were $N_{\text{ap}} = 4$, $n_{\text{SRS}}^{\text{CS,max}} = 12$, $N_{\text{symb}}^{\text{SRS}} = 4$. The entries denote $n_{\text{SRS, eff}}^{\text{CS,i}}$.

| SRS Symbol index | $n_{\text{SRS,eff}}^{\text{CS,0}}$ | $n_{\text{SRS,eff}}^{\text{CS,1}}$ | $n_{\text{SRS,eff}}^{\text{CS,2}}$ | $n_{\text{SRS,eff}}^{\text{CS,3}}$ |
|---|---|---|---|---|
| 11 | 0 | 3 | 6 | 9 |
| 12 | 1 | 4 | 7 | 10 |
| 13 | 2 | 5 | 8 | 11 |
| 14 | 6 | 9 | 0 | 3 |

**TABLE 3.** Example of CS hopping over a subset. Parameters are $N_{\text{ap}} = 2$, $n_{\text{SRS}}^{\text{CS,max}} = 12$, $N_{\text{symb}}^{\text{SRS}} = 4$. The entries denote $n_{\text{SRS, eff}}^{\text{CS,i}}$.

| SRS Symbol index | $n_{\text{SRS,eff}}^{\text{CS,0}}$ UE1 | $n_{\text{SRS,eff}}^{\text{CS,1}}$ UE1 | $n_{\text{SRS,eff}}^{\text{CS,0}}$ UE2 | $n_{\text{SRS,eff}}^{\text{CS,1}}$ UE2 |
|---|---|---|---|---|
| 11 | 0 | 6 | 3 | 9 |
| 12 | 0 | 6 | 5 | 11 |
| 13 | 0 | 6 | 4 | 10 |
| 14 | 0 | 6 | 2 | 8 |

is not configured, that is, there is no CS hopping in a subset. Likewise, comb offset hopping can occur across the entire allowable comb offsets or within a subset of the comb offsets.

We now describe the scheme in detail, as agreed in Release-18. The following can also be found in the official meeting minutes for RAN1 meeting 113. For the SRS hopping formula in CS hopping or comb offset hopping, let $N = 128$, $M = 7$.

- For CS hopping: $\alpha_i = 2\pi\frac{n_{\text{SRS}}^{\text{CS,i}}}{n_{\text{SRS}}^{\text{CS,max}}} + 2\pi\frac{f_{\text{CS, hop}}}{Kn_{\text{SRS}}^{\text{CS,max}}}$ where $f_{\text{CS, hop}} = S\{(\sum_{m}^{M} c(8t+m)2^m) \bmod Y\}$ and
  - $t = (\text{SFN} \bmod N)N_{\text{slot}}^{\text{frame},\mu}N_{\text{symb}}^{\text{slot}} + n_{s,f}^{\mu}N_{\text{symb}}^{\text{slot}} + l_0 + l'$, where SFN, $N_{\text{slot}}^{\text{frame},\mu}$, $N_{\text{symb}}^{\text{slot}}$, $l_0$, $l'$ are all defined in [6].
  - If *cyclicShiftHoppingSubset* is not configured, $S\{n\} = n$, where the $(n+1)$st element of $S$ is denoted by $S\{n\}$
    - If *cyclicShiftHoppingFinerGranularity* is not configured, $Y = n_{\text{SRS}}^{\text{CS,max}}$, $K = 1$
    - If *cyclicShiftHoppingFinerGranularity* is configured, $Y = Kn_{\text{SRS}}^{\text{CS,max}}$, $K = 2$
  - If *cyclicShiftHoppingSubset* is configured, $S\{n\}$ denotes the $(n+1)$st element of the configured subset $S$, $Y$ is the number of elements of the subset and $K = 1$.
- For comb offset hopping: $\bar{k}_0^{(p_i)} = n_{\text{shift}}N_{sc}^{\text{RB}} + (k_{\text{TC}}^{(p_i)} + f_{\text{TC, hop}} + k_{\text{offset}}^{l'}) \bmod K_{\text{TC}}$, where $f_{\text{TC, hop}} = S\{(\sum_{m}^{M} c(8t+m)2^m) \bmod Y\}$ and
  - $t = (\text{SFN} \bmod N)N_{\text{slot}}^{\text{frame},\mu}N_{\text{symb}}^{\text{slot}} + n_{s,f}^{\mu}N_{\text{symb}}^{\text{slot}} + l''$
    - $l'' = l_0 + l'$ if $R = 1$ or UE is provided with *combOffsetHoppingWithRepetition* = per-symbol, otherwise, $l''$ is the OFDM symbol index of the first symbol across the $R$ repetitions within the slot.

- ❏ If *combOffsetHoppingSubset* is not configured, $S\{n\} = n$ and $Y = K_{\text{TC}}$ .
- ❏ If *combOffsetHoppingSubset* is configured, $S\{n\}$ denotes the $(n+1)$st element of the configured subset $S$, and $Y$ is the number of elements in the subset.

When a subset of comb offsets for comb offset hopping is configured and when a subset of CSs for CS hopping is configured, configuring the subset $S = \{S(0), S(1), \ldots, S(z-1)\}$ with $1 < z < Z$, where $Z = K_{\text{TC}}$ for comb offset hopping and $Z = n_{\text{SRS}}^{\text{CS,max}}$ for CS hopping. The quantities $S(0), S(1), \ldots, S(z-1)$ are configured via a $Z$-length bitmap, with $S(i-1)$ being the $i$th bit set as either 0 or 1.

### F. PP-CS SCHEME

Note that in the existing standards [6] and as per the discussion in Sec. I-B, the CSs of all ports are distributed evenly over the range of $0, \ldots, n_{\text{SRS}}^{\text{CS, max}} - 1$. All CS allocations of ports are determined by one parameter $n_{\text{SRS}}^{\text{CS}} \in 0, \ldots, n_{\text{SRS}}^{\text{CS, max}} - 1$ which is contained in the higher layer parameter *transmissionComb*. In the PP-CS allocation scheme, the CS allocation of each port must be configured explicitly by higher-layer messaging. The motivation for this is two-fold, as described below.

First, as described in Sec. I, RAN1 Release-18 standardization assigned a work item for SRS [7], where it was mentioned that *SRS enhancement to manage inter-TRP cross-SRS interference targeting TDD CJT via SRS capacity enhancement and/or interference randomization, with the constraints: 1) without consuming additional resources for SRS, 2) reuse the existing SRS comb structure, and 3) without new SRS root sequences*. Now, let us discuss what it takes to enhance the capacity of SRS. The spacing between the CSs of various ports or UEs depends on the frequency selectivity of the channel. As discussed in Sec. II, the perceived frequency selectivity of the channel is higher than the actual frequency selectivity of the channel, and depends on the type of receiver implementation. In particular, in Fig. 27, it can be seen that the new advanced proposed SRS receiver allows the transmission of six SRSs (with CSs 0,2,4,6,8,10) over 12 subcarriers, which results in better performance than a conventional 3GPP-based SRS receiver based on DFT that supports four SRSs (CSs 0,3,6,9) over 12 subcarriers, as per the 3GPP standard. The six SRSs in question can be a four-port UE (with any four CSs from the set of values of 0,2,4,6,8,10) and a two-port UE (with any two CSs from the set of values of 0,2,4,6,8,10). Note that no two CSs are continuous, and there is a difference of two CS between any two neighbouring CSs. The question inevitably arises, does the standard support such advanced receivers that support closer spacing of CSs than those existing in current standards? If not supported, what needs to be standardized to support such transmissions. The answer is no, such an arrangement can never be supported by the existing standards. The solution to support such advanced receivers and CSs is to be in a position where the CS of each port can be configured individually (hence, the name per-port CS allocation scheme).

Second, consider two two-port UEs: one is a desired UE belonging to a desired TRP and the other is an interfering UE belonging to the interfering TRP. Let us now consider two embodiments. In the first embodiment, the CSs of the desired and interfering UEs are assigned as $d_1 = 0, d_2 = 6, i_1 = 3, i_2 = 9$ and $n_{\text{SRS}}^{\text{CS,max}} = 12$. In the second embodiment, we assigned CSs as $d_1 = 0, d_2 = 3, i_1 = 6, i_2 = 9$ and $n_{\text{SRS}}^{\text{CS,max}} = 12$. Note that in the first embodiment, the CSs are equidistant over $n_{\text{SRS}}^{\text{CS,max}}$ and assigned as per existing standards, whereas in the second embodiment, the CSs are not equidistant over $n_{\text{SRS}}^{\text{CS,max}}$ and can not be configured as per existing standards. In Sec. V, we clearly show that the performance in the second embodiment is much better than that in the first embodiment. Note that in the second embodiment, the CSs of the UE ports must be configured explicitly.

The above two paragraphs provide the motivation for PP-CS scheme.

### G. CONFIGURING SEQUENCE INDEX

This scheme was proposed by [29]. In the existing standards [6], 60 different base sequences with low cross-correlation are defined when the SRS sequence length is equal to or larger than 72 bits by $u = 0, \ldots, 29$ and $v = 0, 1$. However, when sequence hopping is not configured, currently $v$ is always set to zero. This means that out of the 60 base sequences currently defined, only 30 can be assigned to the UEs in the system. With interference planning and when the network carefully assigns SRS parameters to different UEs, allowing the network to configure any of the 60 base sequences can reduce the inter-cluster interference (or even intra-cluster interference, e.g., in the case of a large number of UEs and inside a cluster, other dimensions such as different SRS symbols, different comb offsets, and different CSs are already used). Hence, allowing for the configuration of $v$ per SRS resource is a very simple and yet effective enhancement that makes all the existing 60 different base sequences available for use. Note that this enhancement is not related to interference randomization. Instead, the benefit is enhancing the reuse factor of SRS sequence, that is, more SRS sequences can be configured by the network to ensure that two UEs with the same SRS sequence are far away and do not exhibit clear inter-cell/inter-cluster interference.

### H. LIMITATIONS

In 3GPP standardization, the goal is to obtain as much performance gain as possible with a minimum standardization impact. The SRS receiver, if hardware-based, cannot easily be changed for every release. Therefore, any new proposal is likely to consider possible hardware/implementation changes. If the existing hardware or implementation can support new proposals and show performance gains, such proposals are preferred. On the other hand, if the proposals

are good but may require hardware changes, such proposals may not find much support.

For example, assume that SRS hardware is such that it supports $n_{\text{SRS}}^{\text{CS, max}} = 6, 8, 12$ only as per previous Release-15, Release-16, Release-17, then increasing the maximum number of CSs to beyond the value of 12 may not be preferred, even if it comes with improved performance. If the hardware is such that for a given $n_{\text{SRS}}^{\text{CS, max}}$ and $n_{\text{SRS}}^{\text{CS}}$, it automatically deduces the CSs $n_{\text{SRS}}^{\text{CS, i}}, i = 0, \ldots, N_{ap} - 1$ (as these are evenly spaced in $0, \ldots, n_{\text{SRS}}^{\text{CS, max}} - 1$ as per the existing standards), then supporting the PP-CS scheme is not favourable, as it involves reasonable hardware or implementation changes, even though PP-CS has much better performance. For the same reason, TD-OCC may not be preferred, because it is associated with significant changes. CS and comb hopping may not entail any hardware change, are associated with significant performance improvement, and could be the reason why they were preferred in Release-18 standardization. Perhaps it remains to be seen, for 6G (Release-20), when standardization and SRS receiver design start afresh, if such other proposals can be considered.

## IV. AUTHORS' CONTRIBUTIONS - PP-CS ALLOCATION, CS HOPPING AND MUTING

In this section, we present the motivation for developing the proposed PP-CS allocation scheme. First, we analyse in detail how the frequency selectivity of the channel of the desired and interfering UEs at TRP1 is affected. This is analysed in Sec. IV-A. The conclusions in this section pave the way for the PP-CS allocation scheme proposed in Sec. IV-B.

Referring to Fig. 1, the signal of $\text{UE}_{1,1}$ reaches TRP1 with a zero timing offset owing to the timing advance (TA) concept. Likewise, $\text{UE}_{2,1}$'s signal reaches TRP2 with zero timing offset owing to the timing advance (TA) concept. As TRP1 and TRP2 are synchronized, the UE signals associated with the respective TRPs reach their TRPs at the same time. However, $\text{UE}_{2,1}$'s signal reaches TRP1 with a nonzero timing offset owing to an EPD between the TRPs. This results in a timing offset, which further makes the channel of $\text{UE}_{2,1}$, as seen by TRP1, more frequency selective (the timing offset induces a complex exponential rotation across subcarriers). The detailed analysis is presented in Sec. IV-A.

Normally, if $\text{UE}_{1,1}$ transmits SRS with CS $a$ (no EPD or timing offset), CSs $a-b_1$ to $a + b_1$ (the addition is the modulo operation of the maximum CS, denoted by $n_{\text{SRS}}^{\text{CS,max}}$ in standards) are not used for any other UEs, the value $b_1$ depends on the frequency selectivity of the channel and is called the CS leakage spread (CS-LS) when EPD is zero. However, if $\text{UE}_{2,1}$ transmits SRS with CS $a$ (with an EPD or timing offset at TRP1), CSs $a-b_2-c$ to $a+b_2-c$ are not to be used for any other UEs. The value $b_2$ depends on the frequency selectivity of the channel and $b_2 > b_1, c \geq 0$ (This is due to the EPD of $\text{UE}_{2,1}$'s signal in reaching TRP1.). The value $b_2$ is the CS-LS of an interfering UE with a nonzero EPD or timing offset. The rationale for the above description regarding $b_1, b_2, c$ is discussed in detail in Sec. IV-A. Based on these discussions, we draw important conclusions that form the basis of the PP-CS allocation scheme proposed in Sec. IV-B. Finally, in Sec. IV-C, we present a new muting technique based on the studies conducted in Sec. IV-A and Sec. IV-B, that when used in conjunction with a CS hopping scheme and PP-CS method, removes almost all interference and helps in achieving the lower bound of the no-interference or sTRP case.

### A. ROLE OF EPD FROM UES OF INTERFERING TRPS

Consider an EPD of $x$ for an interfering UE at TRP1. The timing offset of this UE is given by $T_{\text{off}} = \frac{x}{c}$ where $c$ is the speed of light. Let the $12 \times 1$ channel vector across 12 SRS subcarriers in the absence of EPD (we assume maximum CS $n_{\text{SRS}}^{\text{CS, max}} = 12$) be denoted by $\mathbf{h}$. Because of the EPD or timing offset $T_{\text{off}}$, the channel at the $k$th SRS RE or subcarrier is multiplied by $e^{-j2\pi k K_{\text{TC}} \Delta f T_{\text{off}}}$ where the two adjacent SRS REs are separated by $K_{\text{TC}}$ REs and $\Delta f$ is the subcarrier spacing. We see that the effect of timing offset is that the channel at each SRS RE is multiplied by a complex exponential. Define

$$\mathbf{h}_{\text{off}} = \begin{bmatrix} 1 \\ e^{-j2\pi\psi} \\ \vdots \\ e^{-j2\pi 11\psi} \end{bmatrix} \tag{32}$$

where $\psi = K_{\text{TC}} \Delta f T_{\text{off}}$. The effective channel across the SRS subcarriers is denoted as $\bar{\mathbf{h}} = \mathbf{h} \circ \mathbf{h}_{\text{off}}$. Note that $\mathbf{h}$ is a low-pass signal. In a 12-point FFT, bins around zero and 11 are called low-pass bins, and the FFT bins around six are called high-pass bins. The number of low-pass FFT bins on either side (modulo operation) of the DC bin of a low-pass signal (essentially all energy of a low-pass signal is confined to low-pass FFT bins only) will be the same as that of CS-LS. This means that the CS values of two users should at least be separated by two times CS-LS so as not to interfere with each other.

Based on the value of $\psi$ we have the following cases.

- $\psi < \frac{1}{12}$: The CS-LS of $\mathbf{h}$ is $b_1$ and the CS-LS of $\mathbf{h}_{\text{off}}$ is denoted by $b$. The CS-LS of the effective channel is then $b_2 = b_1 + b$ as shown in Fig. 15. This essentially means that CS-LS has increased owing to the EPD, thereby decreasing the capacity of the allowable SRS, as the SRS of two UEs needs to be separated by two times CS-LS. This is depicted in the top-left position of Fig. 13, where the FFT of $\mathbf{h}_{\text{off}}$ for EPD = 100m is denoted. The CS-LS value is $b = 1$. As per the top-left position of Fig. 13, a UE with a CS of $a$ will interfere significantly with another UE transmitting at the CS $(a \pm 1)$ mod 12.
- $\psi$ is a multiple of $\frac{1}{12}$: In this case $\mathbf{h}_{\text{off}}$ is purely a complex exponential (its FFT has just one bin). If $\psi = \frac{1}{12}$, as shown in the top-right portion of Fig. 13, it essentially means that a UE transmitting at CS $a$ is perceived by the TRP as being transmitted with a CS of $(a-1)$ mod 12.

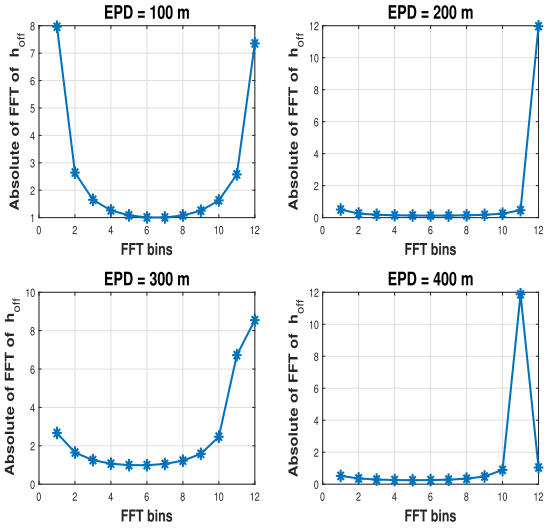


**FIGURE 13.** Absolute of FFT of $\mathbf{h}_{\text{off}}$. $K_{\text{TC}} = 4$, subcarrier spacing = 30 kHz.

In this case, the FFT of $\mathbf{h}$ if cyclically left-shifted by unity, gives the FFT of $\bar{\mathbf{h}}$, as depicted in Fig. 16. In this case, $c = 1$. Similarly, the bottom-right portion of Fig. 13 indicates that a UE transmitting at CS $a$ is perceived by the TRP as being transmitted with a CS of $(a-2)$ mod 12. In this case, the FFT of $\mathbf{h}$ if cyclically left-shifted by two bins gives the FFT of $\bar{\mathbf{h}}$. In this case, $c = 2$ and $\psi = \frac{2}{12}$.

- $\psi > \frac{1}{12}$ and not a multiple of $\frac{1}{12}$: Based on the discussions of above two items, there is an increase in CS-LS $b_2 = b_1 + b$ and also there is a left-shift in CS-LS ($c > 1$). This corresponds to bottom-left part of Fig. 13 and is also depicted in Fig. 17.

Furthermore, Fig. 14 shows that CS-LS increases with an increase in EPD. Based on the preceding discussions, it should be noted that $c > 0$. This is because the effect of the timing offset in the frequency domain $\mathbf{h}_{\text{off}}$ is a low-pass complex exponential signal with a negative frequency $\psi$ (it is assumed that the timing offset $T_{\text{off}}$ is positive). In summary, EPD's effect on a channel is as follows:

- The CS-LS increases due to EPD.
- Interference in the CS domain is always in the left direction ($c > 0$). This can be deduced from Fig. 13. As an example, consider a desired UE's ports as $d_1 = 0, d_2 = 3$ and interfering UE's ports $i_1 = 6, i_2 = 9$ and CS-LS=1. Owing to the EPD of the interfering UE, only the first port of the interfering UE interferes with the second port of the desired UE ($i_1$ interferes with $d_2$) at TRP1. The second port of the interfering UE does not interfere with the first port of the desired UE due to EPD ($i_2$ does not interfere with $d_1$). This is depicted and discussed in detail in Fig. 18.

### B. PROPOSED PP-CS AND LEGACY CS RESOURCE ALLOCATION SCHEMES

Based on the study of the effects of EPD on the channel in the previous subsection, we are now in the position to present the proposed PP-CS method and compare it with the legacy method. As an example, consider one desired UE and one interfering UE, each with two ports (one can also consider

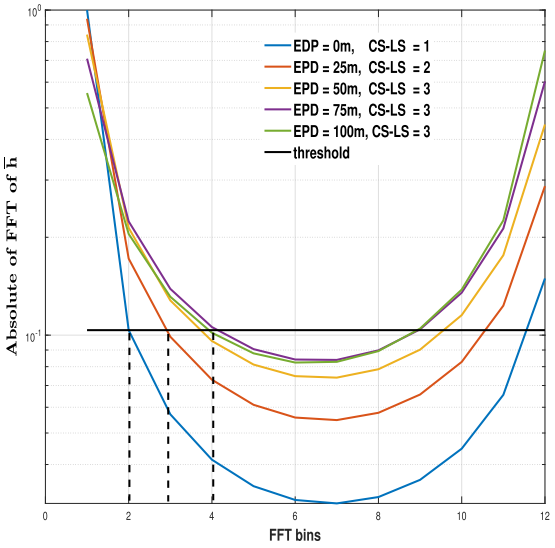


**FIGURE 14.** Absolute of FFT of $\bar{\mathbf{h}}$ (scaled) for different EPD. Depicts the effect of EPD on CS-LS.

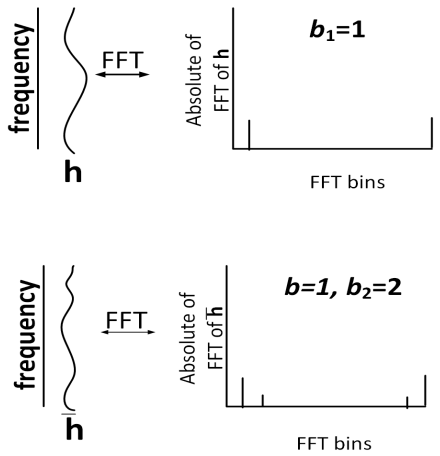


**FIGURE 15.** Absolute of FFT of $\mathbf{h}$ and $\bar{\mathbf{h}}$ when $\psi < \frac{1}{12}$.

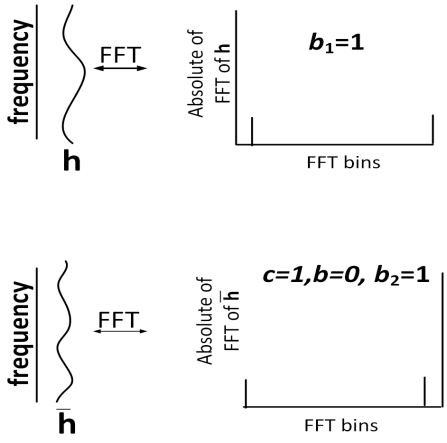


**FIGURE 16.** Absolute of FFT of $\mathbf{h}$ and $\bar{\mathbf{h}}$ when $\psi = \frac{1}{12}$.

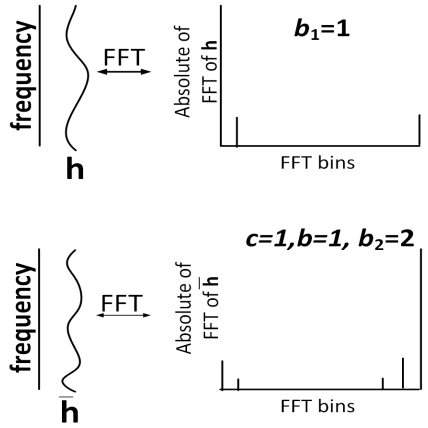


**FIGURE 17.** Absolute of FFT of $\mathbf{h}$ and $\bar{\mathbf{h}}$. $\psi > \frac{1}{12}$ and not a multiple of $\frac{1}{12}$.

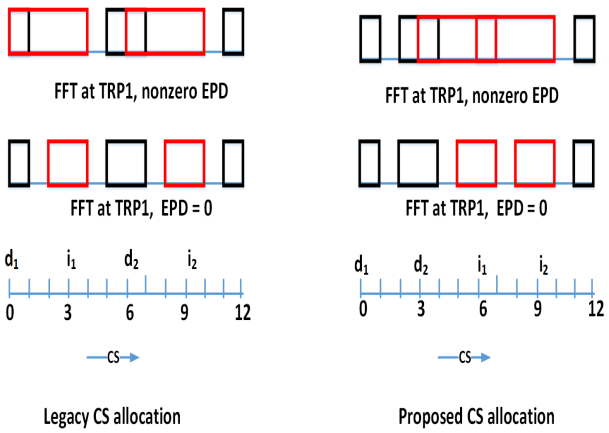


**FIGURE 18.** FFTs of UEs at TRP1. Red boxes denote the FFTs of ports of interfering UEs, whereas black boxes denote FFTs of ports of the desired UE. CS-LS when EPD = 0 is unity ($b_1 = 1$). The other values are $b_2 = 2, b = 1, c = 1$. Legacy CS allocation on the left and, proposed PP-CS allocation on the right.

two desired and two interfering UEs, each with a single port). As an example, consider $n_{\text{SRS}}^{\text{CS,max}} = 12$. As shown in Fig. 18, in the legacy method we assign $d_1 = 0, d_2 = 6, i_1 = 3, i_2 = 9$ while in the proposed method we assign $d_1 = 0, d_2 = 3, i_1 = 6, i_2 = 9$. In the legacy method, the CSs of the ports of the desired UE are interspersed with that of the interfering UE, while in the proposed PP-CS method, the entire CS region of $n_{\text{SRS}}^{\text{CS,max}}$ CSs is divided into two contiguous non-overlapping regions. This region is called as CS region per TRP or CSR-TRP. In the example there are two CSR-TRPs, one is from CSs 0-5, while the second is from CSs 6-11. The first CSR-TRP is allocated to ports of the desired UE, whereas the second CSR-TRP is allocated to the ports of the interfering UE. Within a CSR-TRP, CSs are allocated to the ports of the UE equidistantly. Hence, $d_1 = 0, d_2 = 3, i_1 = 6, i_2 = 9$ are allocated in the proposed method.

In Fig. 18, we show the FFTs of the SRS from both the desired and interfering UEs at TRP1. The CS-LS values are

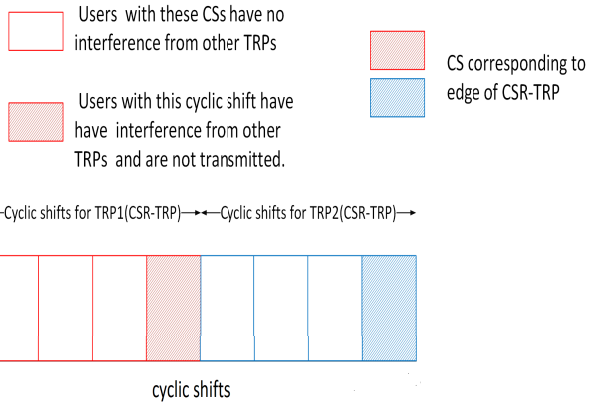


**FIGURE 19.** Depiction of CSR-TRP and muting.

$b_1 = 1, b_2 = 2, b = 1, c = 1$. In the legacy method, all ports $(d_1, d_2)$ of the desired UE experience interference from the interfering UE, whereas in the proposed method, only the ports of the desired UE $(d_2)$ that are at the rightmost edge of the CSR-TRP experience interference, while $d_1$ does not experience any interference. This is confirmed by the simulation results presented in Sec. V-A as well. Hence, the proposed method provides much better immunity against interfering UEs than the legacy method.

### C. CS HOPPING AND MUTING IN THE PROPOSED METHOD

CS hopping is an idea in which CSs are allocated to ports of a UE hop as per a rule across OFDM symbols. The advantage of this method is that the interference observed by a port (user) varies across OFDM symbols, and the channel estimates, which are averaged across OFDM symbols, have an improved SNR. However, the ports remain in the same comb. *CS hopping is a key agreement in Release-18 standardization.*

Muting is a rule in which SRS on some ports is dropped on some occasions or OFDM symbols. Such approaches were discussed in Release-18 [31], [32]. *We present a muting scheme, which in conjunction with the CS hopping scheme and our proposed PP-CS scheme, can remove almost all interference and attain performance comparable to that of an sTRP, which is considered as the lower bound of the mTRP interference case.*

Muting means that as a CS is hopped for a user/port across OFDM symbols, SRS is dropped or not transmitted in those OFDM symbols where the CS is at the edge of CSR-TRP. This is illustrated in Fig. 19. Strictly speaking, muting should not be implemented. The TRP can choose to ignore the SRS in such cases (note that channel estimates are averaged across OFDM symbols and are eventually bad because it averages a bad value when the user is at the rightmost edge of a CSR-TRP with good values when the user is not at the rightmost edge of the CSR-TRP). However, by muting, extra power can be transferred to other ports, which improves the performance.

Muting can be thought of as simple time-division multiplexing (TDM), as follows: Consider the case of four ports (two each from the desired and interfering UEs) to share 12 CSs on a comb in each of the four OFDM symbols with CS hopping and muting. CSR-TRP for the desired UEs comprises CSs 0-5, while CSR-TRP for interfering UEs comprises CSs 6-11. Tables 5 and 6 list examples of CS hopping and muting. Each port has power $P$. Let us consider what occurs in the first SRS symbol. According to the discussion in Sec. IV-B, $d_2$ is at the rightmost edge of the first CSR-TRP and experiences interference from $i_1$ at TRP1 (Refer Fig. 18), whereas $i_2$ is at the rightmost edge of the second CSR-TRP and experiences interference from $d_1$ at TRP2. Therefore, in this OFDM symbol, $d_2$ and $i_2$ are muted and $d_1$ and $i_1$ are transmitted with power $2P$, thereby avoiding interference completely, as ports that are transmitted in this SRS symbol have CSs that are separated by six units (for a delay spread of 100 ns, separation of six CS is more than enough as it is twice the CS-LS). As per the CS hopping and muting example in Table 6, each port is transmitted only for two OFDM symbols but with a power $2P$ whereas without muting, they are transmitted in all four OFDM symbols with a power $P$. The reduced processing gain owing to each user being present in only half of the OFDM symbols is well compensated by increasing the power to twice the usual value. Another perspective is as follows: Ideally speaking, since only UE/ports that have a CS at the rightmost edge of a CSR-TRP experience interference, we can avoid such interference by having a guard band of CSs (no UEs/ports are assigned CSs in this guard band) between two adjacent CSR-TRPs. However, this proves costly because we have only a small region of 12 maximum CSs. So muting can be thought of having a guard band of CSs between the effective CSR-TRPs (The effective CSR-TRP is the actual CSR-TRP region minus the muted CS region at the rightmost edge of the CSR-TRP).

## V. SIMULATION RESULTS

In the simulations, the CDL-C [33] reference channel model with a subcarrier spacing 30 kHz, UE speed = 3km/hr, and carrier frequency 3.5 GHz are considered. The antenna configuration at the TRP consists of 16 antenna ports and is given by $(M = 8, N = 4, P = 2, Mg = 1, Ng = 1, Mp = 2, Np = 4)$. The antenna spacing in the horizontal and vertical directions is given by (dH,dV) = (0.5, 0.8)$\lambda$, where $\lambda$ denotes the wavelength of the carrier. The configuration of the UE antenna is omnidirectional. We assumed four SRS symbols in a slot and $K_{\text{TC}} = 4$ and $n_{\text{SRS}}^{\text{CS,max}} = 12$. Unless otherwise mentioned, the performance measure is the normalized channel estimation error (NCEE) (defined subsequently) which is computed across all combs, and the channel is interpolated across combs that do not carry the SRS of the desired and interfering UEs. NCEE is always calculated only for the channels of the desired UEs. We consider one multi-port desired UE and one multi-port interfering UE for the mTRP scenario. In the following figures, we compare the mTRP scenario (which has both desired and interfering UEs) with the sTRP scenario (that has only desired UEs and no interference or interfering UEs) which serves as a low bound for the mTRP scenario.

### A. PP-CS SCHEMES

The following scenarios are studied and compared.

1) **Legacy CS allocation, no CS hopping:** The same CS allocation is used across the four SRS symbols. Two delay spreads (DS) of 30 ns and 100 ns were studied. Figs. 20 and 21 correspond to three-port UEs (Standards do not speak about three-port UEs, we study them for comparison purposes only) and have CSs $d_1 = 0, d_2 = 4, d_3 = 8, i_1 = 2, i_2 = 6, i_3 = 10$. Figs. 22 and 23 correspond to two-port UEs and have CSs $d_1 = 0, d_2 = 6, i_1 = 3, i_2 = 9$.
2) **roposed PP-CS allocation, no CS hopping:** The same CS allocation is used across the four SRS symbols. Two delay spreads of 30 ns and 100 ns were studied. Figs. 20 and 21 correspond to three-port UEs and have CSs $d_1 = 0, d_2 = 2, d_3 = 4, i_1 = 6, i_2 = 8, i_3 = 10$. Figs. 22 and 23 correspond to two-port UEs and have CSs $d_1 = 0, d_2 = 3, i_1 = 6, i_2 = 9$.
3) **Legacy CS allocation with CS hopping:** The CS allocation is shown in Table 4 and studied in Fig. 24.
4) **Proposed PP-CS allocation scheme with CS hopping:** The CS allocation is shown in Table 5 and studied in Fig. 24.
5) **Proposed PP-CS allocation scheme with CS hopping and muting:** The CS allocation is shown in Table 6 and studied as shown in Fig. 25. In this scheme, in any OFDM symbol, the port associated with a CS that is at the edge of the CSR-TRP (CSs of three or nine) will not transmit any SRS (be on mute).

The performance measure is NCEE, defined as

$$\text{NCEE} = \frac{\sum_{i=0}^{N_U-1} E\{|\mathbf{h}_i - \hat{\mathbf{h}}_i|^2\}}{\sum_{i=0}^{N_U-1} E\{|\mathbf{h}_i|^2\}}. \tag{33}$$

Note that the NCEE has no units. In the legends for the figures, a mention of $d_1$ means that it is the performance of $d_1$, and a mention of $d_1, d_2$ means that it is the performance of either of $d_1$ or $d_2$. The following description of graphs for PP-CS-related figures is used to quickly identify various scenarios in the plots.

- Black colour for legacy CS allocation.
- Blue colour for proposed PP-CS allocation.
- Red colour for the case of sTRP, no interference case. This serves as a lower bound for the mTRP.
- Solid line means no hopping.
- Dashed line means hopping and/or muting.

This is discussed further in Sec. IV-B where only the ports that are at the rightmost edge of a CSR-TRP experience interference from UEs belonging to other TRP. We now depict the results for the same. Fig. 21 depicts the NCEE of the legacy and the proposed CS allocation schemes with no

hopping. As it corresponds to a low delay spread, we have three ports in the CSR-TRP. Based on Fig. 21, we can observe the effect of interference depending on the CS value of each port. For the PP-CS scheme, it can be seen that the performance of $d_3$, whose CS is at the rightmost edge of the CSR-TRP, is affected by the interference from the UEs of the other TRP, while the performance of $d_1, d_2$, whose CS is away from the rightmost edge of the CSR-TRP, is hardly affected by the interference from the UEs of the other TRPs. For the proposed PP-CS, the NCEE of $d_3$ (at a high SNR) was approximately 1.5% higher than that of $d_1, d_2$. Furthermore, the NCEE of the proposed PP-CS (for $d_1, d_2$) is approximately 1.5% lower than that of the legacy (conventional) scheme at a high SNR. In the PP-CS scheme, ports $(d_1, d_2)$ have similar performances to the case of sTRP (no interference scenario). The proposed PP-CS allocation ensures good performance for $d_1, d_2$, whereas $d_3$ is impaired and has poor performance, which is better than the case of legacy CS schemes where all $d_1, d_2, d_3$ achieve poor performance. A similar result is observed in Fig. 23, where a higher delay spread of 100 ns allows us to accommodate only two ports in the CSR-TRP. The NCEE of the proposed PP-CS for port $d_1$ is approximately 9% less than that of the legacy (conventional) method. Furthermore, it should be noted that the benefits of the proposed method, compared to legacy methods, appear only in cases with significant EPD for a given delay spread. In the above figures, for values of EPD=225 m for a delay spread of 100 ns and EPD = 120 m for a delay spread of 30 ns, the proposed method was better than the legacy method. For EPDs less than these, as shown in Figs. 20 and 22, the impact of EPD is negligible and hardly any interference due to these EPDs exists (all performances are similar).

Fig. 24 shows that CS hopping in conjunction with the legacy method is better than the legacy method with no CS hopping. Similarly, it also shows that CS hopping in conjunction with the proposed PP-CS method is better than the proposed PP-CS method with no hopping. We can see that the NCEE (at a high SNR) of CS hopping in conjunction with the legacy method is approximately 50% less than that of the legacy method with no CS hopping. Likewise, the NCEE (at a high SNR) of CS hopping in conjunction with the proposed PP-CS is approximately 80% less than that of the legacy method with no hopping. Furthermore, it shows that the performance of CS hopping in the context of the proposed PP-CS method is better than CS hopping in the context of the legacy method. We can see that the NCEE (at a high SNR) of CS hopping in the context of the proposed PP-CS is 30% less than that associated with CS hopping in the context of the legacy method. *Fig. 25 shows that the proposed PP-CS method with CS hopping and muting achieves a lower-bound performance of the no-interference sTRP case*. We can see that for the proposed PP-CS scheme, NCEE (at a high SNR) is reduced by almost 90% owing to CS hopping, while it is reduced by almost 99% because of CS hopping and muting (compared to the case of PP-CS with no hopping and muting).

**TABLE 4. Legacy CS allocation with hopping.**

| SRS Symbol index | $d_1$ | $d_2$ | $i_1$ | $i_2$ |
|---|---|---|---|---|
| 11 | 0 | 6 | 3 | 9 |
| 12 | 0 | 6 | 9 | 3 |
| 13 | 6 | 0 | 3 | 9 |
| 14 | 6 | 0 | 9 | 3 |

**TABLE 5. Proposed PP-CS allocation with hopping.**

| SRS Symbol index | $d_1$ | $d_2$ | $i_1$ | $i_2$ |
|---|---|---|---|---|
| 11 | 0 | 3 | 6 | 9 |
| 12 | 0 | 3 | 9 | 6 |
| 13 | 3 | 0 | 6 | 9 |
| 14 | 3 | 0 | 9 | 6 |

**TABLE 6. Proposed PP-CS allocation with hopping and muting.**

| SRS Symbol index | $d_1$ | $d_2$ | $i_1$ | $i_2$ |
|---|---|---|---|---|
| 11 | 0 | No SRS | 6 | No SRS |
| 12 | 0 | No SRS | No SRS | 6 |
| 13 | No SRS | 0 | 6 | No SRS |
| 14 | No SRS | 0 | No SRS | 6 |

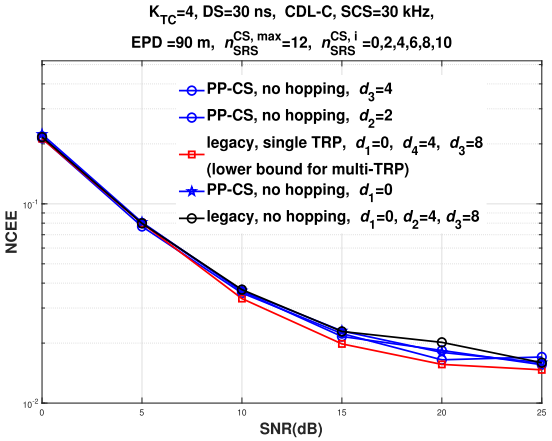


**FIGURE 20. Performance comparisons of legacy and proposed PP-CS methods, no hopping. Delay spread = 30 ns, EPD = 90 m. Three-port desired and interfering UEs are considered. mTRP is considered. NCEE has no units.**

### B. CAPACITY ENHANCEMENT

In Fig. 26, it is shown that the new advanced SRS receiver proposed in Sec. II, which is based on Slepian/polynomial basis has at least 5 dB gain (at NCEE of 0.04) as compared to the conventional SRS receivers based on DFT. At high SNR, the new advanced proposed SRS receiver from Sec. II, that is based on Slepian/polynomial basis has an NCEE that is less by an order of magnitude (from $10^{-2}$ to $10^{-3}$) as compared to the conventional SRS receivers based on DFT.

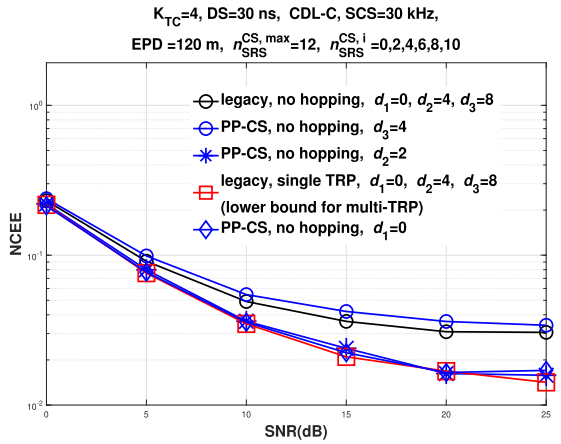


**FIGURE 21.** Performance comparisons of legacy and proposed PP-CS methods, no hopping. Delay spread = 30 ns, EPD = 120 m. Three-port desired and interfering UEs are considered. mTRP is considered.

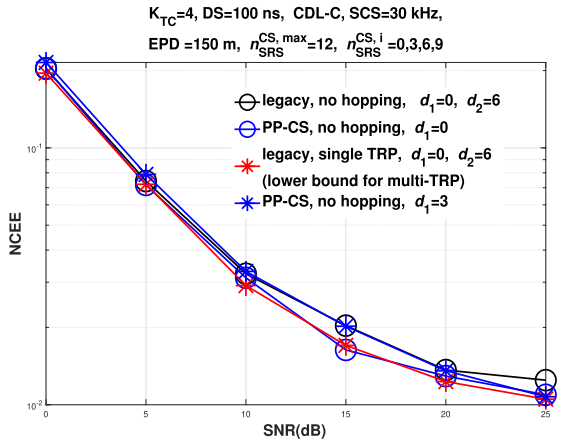


**FIGURE 22.** Performance comparisons of legacy and proposed PP-CS methods, no hopping. Delay spread = 100 ns, EPD = 150 m. Two-port desired and interfering UEs are considered. mTRP is considered.

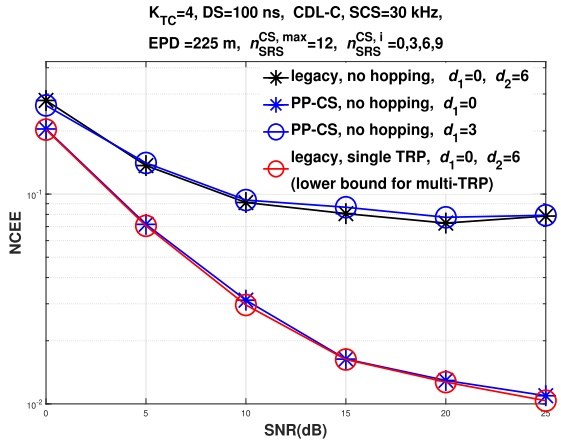


**FIGURE 23.** Performance comparisons of legacy and proposed PP-CS methods, no hopping. Delay spread = 100 ns, EPD = 225 m. Two-port desired and interfering UEs are considered. mTRP is considered.

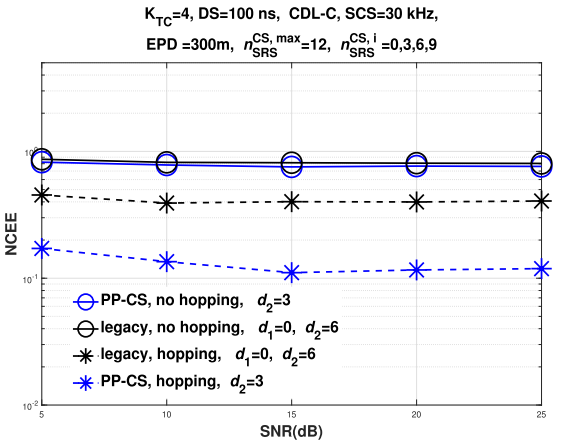


**FIGURE 24.** Performance comparisons of legacy and proposed PP-CS methods with hopping. Delay spread = 100 ns, EPD = 300 m. Two-port desired and interfering UEs are considered. mTRP is considered.

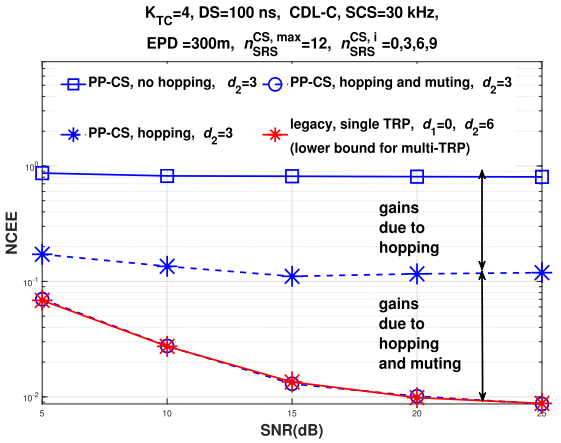


**FIGURE 25.** Performance comparisons of legacy and proposed PP-CS methods with hopping and muting. Delay spread = 100 ns, EPD = 300 m. Two-port desired and interfering UEs are considered. mTRP is considered.

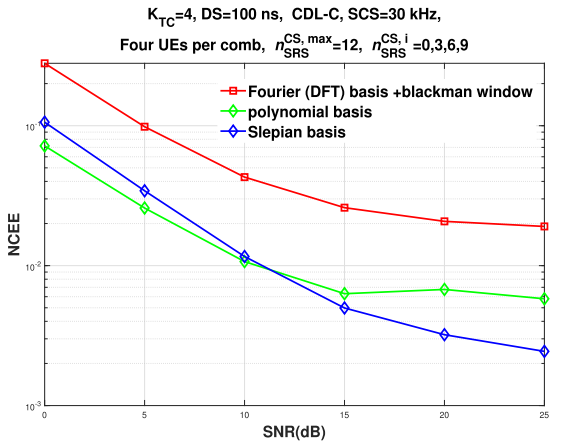


**FIGURE 26.** Performance comparisons of conventional DFT-based and proposed Slepian/polynomial-based SRS receiver with $N_U = 4$ and associated CSs 0,3,6,9. sTRP is considered. Only the comb that carries $N_U$ SRS is considered.

We attempt to trade of performance improvement for capacity enhancement. In Fig. 27, it can be seen that the new advanced proposed SRS receiver allows transmission of six SRSs over 12 subcarriers which results in better performance (at least greater than 5 dB gain at NCEE of 0.04) than a conventional SRS receiver based on DFT that supports four SRSs over 12 subcarriers as per the 3GPP standard.

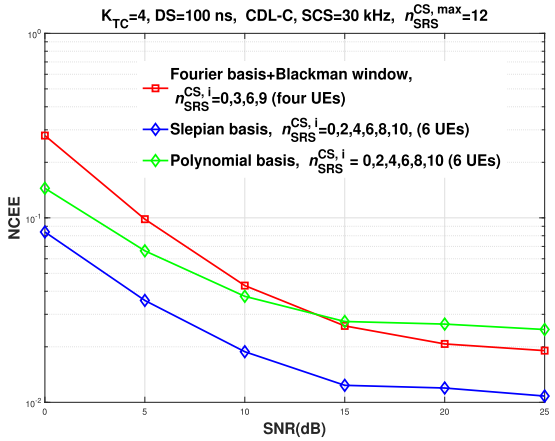


**FIGURE 27.** Performance comparisons of conventional DFT-based and proposed Slepian/polynomial-based SRS receiver with $N_U = 4$ and associated CSs 0,3,6,9 for the conventional receiver and $N_U = 6$ and associated CSs 0,2,4,6,8,10 for the proposed receiver. sTRP is considered. Only the comb that carries $N_U$ SRS is considered.

### C. IMPACT ON 5G RAN1 STANDARDIZATION

In the mTRP operation in 5G, as seen in [3], the SRSs of UEs experience interference, which can come in the way of realizing the promised gains of cell-free massive MIMO. Therefore, it is very important to address the challenges of reducing and managing the interference associated with SRS. As discussed in [3], current approaches to handle interference, such as whitening, are insufficient. To this end, many approaches have been investigated, and our proposed CS hopping scheme in the context of legacy systems (that was accepted in Release-18 standardization) significantly reduces interference (we also proposed CS hopping in the context of our proposed PP-CS scheme with much better performance than CS hopping in the context of legacy systems), as can be seen from the discussions in Sec. V and Fig. 24 and Fig. 25. This effective means of reducing interference and improving SRS channel estimates helps improve the overall performance in 5G and achieve the promised gains of cell-free massive MIMO.

For better performance, we would want to serve as many UEs as possible. Therefore, we are always looking at improvements in the capacity of SRS. As more SRSs are accommodated with the intention of improved capacity, performance has a hit. Improving capacity means accommodating the SRSs closer to each other in the CS domain, which depends on leakages. These leakages were shown to be high for the DFT-based receivers. We proposed Slepian-based SRS receivers that minimize these leakages, thereby improving their capacity. To realize this improved capacity, the PP-CS scheme should be used, as discussed in Sec. II-F. If the PP-CS scheme is not used, to exploit the advantages of the proposed SRS receiver, the capacity improvement can be traded with the performance improvement, as shown in Fig. 26. The uplink performance of SRS is also closely linked to the uplink transmission power, which in turn is also linked to cell coverage. Our proposed SRS receivers will improve the SRS performance significantly, resulting in realising as much as possible of the promised gains in cell-free massive MIMO for upcoming 5G systems.

## VI. CONCLUSION

The SRS work item in 3GPP Release-18 for the TDD CJT for mTRPs has two parts. The first was IRT and the second was CE. We have provided a brief summary and overview, along with corresponding references for the various IRT of SRS interference management for TDD CJT work items discussed in Release-18 standardization. In this context, we explain our PP-CS scheme in detail. We have shown that the PP-CS scheme, along with CS hopping and muting, can achieve a lower bound in performance for the case of no interference or the sTRP method.

For the CE part of Release-18, we present a new Slepian / polynomial-based SRS receiver that supports six SRSs and has a better performance than the conventional DFT-based SRS receivers based on the 3GPP standard, which supports only four SRSs. We discuss the necessary changes that need to be made to the standards to support such improved SRS receivers.

Finally, we have this to say about the future work. It was shown that the capacity of SRS was significantly affected by leakages, increasing the perceived bandwidth, which was greater than the true bandwidth of an SRS channel. This is mainly due to the small number of SRS subcarriers. It was also shown that leakages were reduced and perceived bandwidth was almost the same as the true bandwidth of an SRS channel as the number of SRS subcarriers increased. This is the motivation to increase the CS and maximum CS values. This can be further investigated, and as part of this investigation, one can see whether the performance and capacity improvements of Slepian-based SRS receivers over conventional DFT-based receivers are impacted or not, with an increase in maximum CS values, for the case when number of SRS subcarriers are high. Furthermore, we can also investigate the impact of small timing offsets (timing offsets are usually small owing to timing advance features) on the Slepian-based SRS receiver. We showed the performance and capacity improvements in the frequency domain only. Such improvements are also possible in the time domain when mobility is present. Therefore, the joint architecture of Slepian-based SRS in both time and frequency can be explored next. Note that in the time domain, this would mean some form of TD-OCC, and will also have similarities with orthogonal time frequency space (OTFS) modulation schemes. Finally, more detailed investigations of the PP-CS method can be carried out to ascertain its usefulness in future 3GPP standardization activities.

## REFERENCES

[1] H. Q. Ngo, A. Ashikhmin, H. Yang, E. G. Larsson, and T. L. Marzetta, "Cell-free massive MIMO versus small cells," *IEEE Trans. Wireless Commun.*, vol. 16, no. 3, pp. 1834–1850, Mar. 2017.

[2] E. Björnson and L. Sanguinetti, "Making cell-free massive MIMO competitive with MMSE processing and centralized implementation," *IEEE Trans. Wireless Commun.*, vol. 19, no. 1, pp. 77–90, Jan. 2020.

[3] H. Jin, K. Liu, M. Zhang, L. Zhang, G. Lee, E. N. Farag, D. Zhu, E. Onggosanusi, M. Shafi, and H. Tataria, "Massive MIMO evolution toward 3GPP release 18," *IEEE J. Sel. Areas Commun.*, vol. 41, no. 6, pp. 1635–1654, Jun. 2023.

[4] E. G. Larsson, O. Edfors, F. Tufvesson, and T. L. Marzetta, "Massive MIMO for next generation wireless systems," *IEEE Commun. Mag.*, vol. 52, no. 2, pp. 186–195, Feb. 2014.

[5] T. L. Marzetta, "Massive MIMO: An introduction," *Bell Labs Tech. J.*, vol. 20, pp. 11–22, 2015.

[6] *Physical Channels and Modulation*, Standard TS 38.211, V17.0.0, 3GPP, 2021.

[7] *New WID: MIMO Evolution for Downlink and Uplink*, Standard RP-213598, 2021.

[8] X. Hou, C. Na, and A. Harada, "Investigation on multi-cell sounding reference signal coordination for TD-LTE-advanced CoMP," in *Proc. IEEE 77th Veh. Technol. Conf.*, Jun. 2013, pp. 1–5.

[9] L. R. Costa, D. C. Moreira, S. Sandberg, A. Simonsson, and Y. C. B. Silva, "Interference mitigation based on precoded SRS," in *Proc. IEEE Sensor Array Multichannel Signal Process. Workshop (SAM)*, Jul. 2016, pp. 1–5.

[10] Y. Si, Y. Zheng, S. Ren, and J. Wu, "Interference cancellation and coordination scheme for sounding reference signal in multiple-beam mobile satellite communication system," in *Proc. IEEE 75th Veh. Technol. Conf.*, Yokohama, Japan, May 2012, pp. 1–5.

[11] B. Ghimire, E. Eberlein, and M. Alawieh, "Reference signal enhancement in 5G for extended coverage in multi-user scenarios," in *Proc. IEEE 96th Veh. Technol. Conf.*, Sep. 2022, pp. 1–6.

[12] X. Hou, Z. Zhang, and H. Kayama, "DMRS design and channel estimation for LTE-advanced MIMO uplink," in *Proc. IEEE 70th Veh. Technol. Conf. Fall*, Sep. 2009, pp. 1–5.

[13] P. Bertrand, "Channel gain estimation from sounding reference signal in LTE," in *Proc. IEEE 73rd Veh. Technol. Conf.*, May 2011, pp. 1–5.

[14] T. Zemen and C. F. Mecklenbrauker, "Time-variant channel estimation using discrete prolate spheroidal sequences," *IEEE Trans. Signal Process.*, vol. 53, no. 9, pp. 3597–3607, Sep. 2005.

[15] D. Slepian and H. O. Pollak, "Prolate spheroidal wave functions, Fourier analysis and uncertainty—I," *Bell Syst. Tech. J.*, vol. 40, no. 1, pp. 43–63, Jan. 1961.

[16] J. Kim, C.-W. Wang, and W. E. Stark, "Frequency domain channel estimation for OFDM based on slepian basis expansion," in *Proc. IEEE Int. Conf. Commun.*, Jun. 2007, pp. 3011–3015.

[17] P. S. Rossi and R. R. Müller, "Slepian-based two-dimensional estimation of time-frequency variant MIMO-OFDM channels," *IEEE Signal Process. Lett.*, vol. 15, pp. 21–24, Sep. 2008.

[18] J. Mathews, J. Breakall, and G. Karawas, "The discrete prolate spheroidal filter as a digital signal processing tool," *IEEE Trans. Acoust., Speech, Signal Process.*, vols. ASSP-33, no. 6, pp. 1471–1478, Dec. 1985.

[19] T. Zemen, C. F. Mecklenbrauker, F. Kaltenberger, and B. H. Fleury, "Minimum-energy band-limited predictor with dynamic subspace selection for time-variant flat-fading channels," *IEEE Trans. Signal Process.*, vol. 55, no. 9, pp. 4534–4548, Sep. 2007.

[20] M. A. Davenport and M. B. Wakin, "Compressive sensing of analog signals using discrete prolate spheroidal sequences," 2012, *arxiv:1109.3649*.

[21] Y. Zhang, *Sounding Reference Signal Resource Capacity Enhancement for Wireless Communications*, Standard WO2021203271, 2021.

[22] K. Muralidhar, "System and method for accommodating more number of users over resource blocks in an uplink transmission," U.S. Patent 11 206 165, Dec. 7, 2021.

[23] Z. Tang, R. Claudio Cannizzaro, G. Leus, and P. Banelli, "Pilot-assisted time-varying channel estimation for OFDM systems," *IEEE Trans. Signal Process.*, vol. 55, no. 5, pp. 2226–2238, May 2007.

[24] D. K. Borah and B. T. Hart, "Frequency-selective fading channel estimation with a polynomial time-varying channel model," *IEEE Trans. Commun.*, vol. 47, no. 6, pp. 862–873, Jun. 1999.

[25] *On SRS Enhancement*, Standard R1-2206191, Google, 2022.

[26] *Discussion on SRS Enhancements*, Standard R1-2206624, Xiaomi, 2022.

[27] *SRS Enhancements for TDD CJT and 8TX Operation*, Standard R1-2205750, Futurewei, 2022.

[28] *SRS Enhancement for TDD CJT and UL 8Tx Operation in Rel-18*, Standard R1-2205883, Huawei, 2022.

[29] *SRS Enhancement for TDD CJT and 8 Tx Operation*, Standard R1-2301399, Qualcomm, 2022.

[30] *Discussion on SRS Enhancement for TDD CJT and UL 8Tx Operation in Rel-18*, Standard R1-2306537, Huawei, 2023.

[31] *SRS Enhancement Targeting TDD CJT and 8 TX Operation*, OPPO Standard R1-2211429, 2022.

[32] *Views on SRS Enhancements*, Standard R1-2301251, Samsung, 2022.

[33] *Study on Channel Model for Frequencies From 0.5 To 100 GHz*, Standard TR 38.901, V17.0.0, 3GPP, 2022.

[34] *SRS Enhancement Targeting TDD CJT and 8 TX Operation*, Standard R1-2211429, OPPO, 2022.

[35] *Discussion of SRS Enhancement*, Standard R1-2211294, Lenovo, 2022.

[36] *Discussion on SRS Enhancement Targeting TDD CJT and 8 TX Operation*, Standard R1-2211668, CMCC, 2022.

[37] *SRS Enhancement Targeting TDD CJT and 8 TX Operation*, Standard R1-2306613, ZTE, 2023.

[38] *On SRS Enhancements Targeting TDD CJT and 8 TX Operation*, Standard R1-2306807, Ericsson, 2023.

[39] *SRS Enhancements for TDD CJT and 8TX Operation*, Standard R1-2306424, Futurewei, 2023.

[40] *SRS Enhancements for TDD CJT and 8TX Operation*, Standard R1-2300051, Futurewei, 2022.


**KARTHIK MURALIDHAR** received the master's degree from IIT Kanpur, India, in 2009, and the Ph.D. degree from Nanyang Technological University, Singapore, in 2010. He joined Samsung Research and Development Institute, Bengaluru, India, in 2021, where he has been involved in 3GPP RAN1 standardizations. His research interests include massive MIMO, compressed sensing, and AI-ML.

**YOUNGROK JANG** received the B.S. and Ph.D. degrees in electrical and electronic engineering from Yonsei University, Seoul, South Korea, in 2012 and 2019, respectively. He joined Samsung Electronics, in 2019, where he has been involved in 3GPP RAN1 standardizations. His current research interests include massive MIMO, full duplex, and machine learning-based wireless communication systems.

**YOUNSUN KIM** (Senior Member, IEEE) joined Samsung in 1999, where he has been involved on cellular communications standards for over 20 years. He has contributed to critical advancements on physical layer technologies, such as network coordination, MIMO, duplex, and network energy savings. He is currently the Chair of 3GPP RAN1, which is tasked with the development of physical layer technologies for 3GPP specifications.

**DIWAKAR SHARMA** received the B.Tech. degree in computer engineering from Jiwaji University, India, in 1999. He is currently pursuing the Ph.D. degree in wireless communication with IIIT-Bengaluru, India. He has been associated with Samsung, India, since 2000, and involved in development of system engineering and research of physical layer for 4G and 5G. He is also contributing to 3GPP standardization efforts from Samsung. His research interests include wireless communications, MIMO schemes, and optimization issues.

**HYOUNG-JU JI** (Senior Member, IEEE) received the Ph.D. degree in electrical engineering from Seoul National University. He joined Samsung Electronics, in 2007, where he has been involved in 3GPP RAN1 standardizations. He is currently a Principal Engineer with Samsung Electronics. His current research interests include advanced duplex scheme, multi-antenna techniques, and compressed sensing.

**SANTANU MONDAL** received the B.Tech. degree (Hons.) in electronics and electrical communication engineering from Indian Institute of Technology at Kharagpur, Kharagpur, India, in 2010, and the M.Sc. (Engg.) degree in electrical communication engineering from Indian Institute of Science, Bengaluru, India, in 2013. He joined Samsung Research and Development Institute, in 2021, where he has been involved in 3GPP RAN1 standardization. Previously, he was with Qualcomm and Mavenir, wherein he was involved in system design and algorithm development for IEEE 802.11ac/ax and LTE/5G-NR systems, respectively. His current research interests include massive MIMO, full-duplex, integrated sensing and communication, and machine learning-based wireless communication systems.

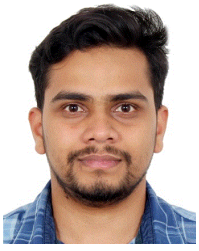

**DATTARAJ DILEEP RAUT MULGAONKAR** received the B.E. degree in electronics and telecommunication engineering from Goa University, Goa, India, in 2016, and the master's degree in communication engineering from BITS-Pilani, Rajasthan, India, in 2019. He joined Samsung Research and Development Institute, Bengaluru, India, in 2019, where he has been involved in regional spectrum simulations and 3GPP RAN1 standardizations. His current research interests includes massive MIMO.

**SATYA KUMAR VANKAYALA** (Senior Member, IEEE) received the master's degree from Indian Institute of Technology at Guwahati, Guwahati, India, in 2008, and the Ph.D. degree from Indian Institute of Science, Bangalore, India, in 2018. He is currently an Architect with Samsung Research and Development Institute, Bengaluru, India. He has filed more than 30 U.S. patents and published more than 35 papers in various reputed conferences. In 2016, he received the Best White Paper Award from Nokia Bell Labs in research category, the Best Paper Award in 2021 WPMC, Japan, and the Best Paper Award in IEEE ANTS, 2022. He received the Zinnov Industry Award in 2021, in mid level experience category for his innovations.

**SEONGMOK LIM** received the B.S. and Ph.D. degrees in electronic engineering from Yonsei University, Seoul, South Korea, in 2013 and 2019, respectively. He joined Samsung Electronics, in 2019, where he has been involved in 3GPP RAN1 standardizations. His current research interests include massive MIMO and signal processing for direction finding.